ADVANCED NANOBIOMED RESEARCH Open Access
www.advnanobiomedres.com

Stimuli-Responsive Dendritic Supramolecular Vector for Tumor-Specific Gene Delivery

Xumei Ouyang, Dongruo Gao, Jie Shen, Yichen Zhou, Ying Gao, Yuanyuan Lv, Qiwen Wang,* Guocan Yu,* and Paul K. Chu**

To simplify the preparation of dendritic materials, host–guest molecular recognition and self-assembly are utilized to form a supramolecular dendritic gene vector (DNCVP). DNCVP is constructed from an amino dendron-conjugated naphthol, viologen containing pH-sensitive hydrazone-bond-linked PEG, and CB[8] with a molar ratio of 1:1:1. The pH- and reducing-sensitivity of DNCVP is verified, and the stimuli-responsive capacity enables the vector tumor targeting gene delivery ability. Owing to the protection of surface PEG, the supramolecular engineering endows the delivery vector with low cytotoxicity and good biocompatibility that are confirmed by the MTT assay. The excellent delivery ability of genes is investigated by in vitro transfection of pEGFP, pGL3, and silencing of siGAPDH. In vivo studies demonstrate promoted tumor accumulation of genes mediated by the dual-responsive DNCVP and the transfection efficiency at the tumor site is greatly improved benefiting from the dynamic nature of noncovalent interactions. This study reveals DNCVP is a promising supramolecular dendritic gene delivery vector, providing a sophisticated strategy for precise gene therapy.

1. Introduction

Gene therapy is vital to cancer treatment and current methods for gene delivery involve viral and nonviral vectors.[1] Synthetic materials as nonviral gene delivery vectors exhibit the advantages of low immunogenicity, changeable structure, and ease of modification thus facilitating safe delivery of gene drugs.[2] Dendrimers are a unique class of nanoscale macromolecules with regular and size-controllable 3D architectures,[3] and the abundant functional groups on the surface allow optimization of dendrimers to cater to specific applications by modifying with different functional moieties.[4] These features endow them with the structural basis for the ideal gene carriers, thus dendrimers are widely used in tumor-targeting gene or drug delivery.[5] However, application of conventional dendrimers faces obstacles including the efficacy of turbulent transfection as the different generation and

X. Ouyang, D. Gao, J. Shen, Y. Zhou, Y. Gao, Y. Lv
Key Laboratory of Novel Targets and Drug Study for Neural Repair of Zhejiang Province
School of Medicine
Hangzhou City University
Hangzhou 310015, China
E-mail: shenj@zucc.edu.cn

X. Ouyang
Guangdong Provincial Key Laboratory of Tumor Interventional Diagnosis and Treatment
Zhuhai Institute of Translational Medicine Zhuhai People's Hospital Affiliated with Jinan University
Jinan University
Zhuhai, Guangdong 519000, China

X. Ouyang, J. Shen, Y. Gao, Y. Lv
Institute of Pharmaceutics, College of Pharmaceutical Sciences
Zhejiang University
Hangzhou 310058, China

The ORCID identification number(s) for the author(s) of this article can be found under https://doi.org/10.1002/anbr.202200172.

DOI: 10.1002/anbr.202200172

D. Gao, Y. Lv
College of Chemical and Biological Engineering
Zhejiang University
Zhejiang, Hangzhou 310027, China

Q. Wang
Department of Cardiology
The First Affiliated Hospital
School of Medicine
Zhejiang University
Hangzhou 310003, China
E-mail: wangqiwen@zju.edu.cn

G. Yu
Key Laboratory of Bioorganic Phosphorus Chemistry & Chemical Biology
Department of Chemistry
Tsinghua University
Beijing 100084, China
E-mail: guocanyu@mail.tsinghua.edu.cn

J. Shen, P. K. Chu
Department of Physics
Department of Materials Science and Engineering, and Department of Biomedical Engineering
City University of Hong Kong
Tat Chee Avenue, Kowloon, Hong Kong, China
E-mail: paul.chu@cityu.edu.hk

structure, unsatisfactory blood circulation lifetime, and insufficient intratumoral accumulation.[6] Therefore, it is crucial to overcome these limitations by functional modification of dendrimers.

In recent years, the concept of precision medicine has become a trendsetter in disease treatment and the smart drug delivery system, an important strategy for precision drug delivery with the goal of delivering medications to disease lesions as well as judging and responding to special stimulation conditions in the environments to accomplish on/off drug release control, is receiving more and more attention.[7] Dendrimers have shown distinct therapeutic advantages in tumor treatment as smart responsive carriers.[8] Various modified dendrimers have been created by alteration of surface functional groups to enrich the stimuli-responsive capabilities, enhance in vivo processes, and eventually boost the delivery efficiency.[9] However, chemical linkage is required to introduce multiple functional segments to the dendrimer to accomplish high stability, good biocompatibility, effective gene payload, and multiple stimulus responses.[10] Therefore, the synthesis processes may suffer from cumbersome synthetic manipulation, tedious purification, and poor overall yield after multistep functionalization.[11] In this respect, supramolecular chemistry provides insights into tackling the task.

Benefiting from the dynamic and reversible nature of supramolecular chemistry, stable and ordered complex systems can be formed through noncovalent interactions-mediated self-assembly, especially for host–guest recognitions.[12] This technique allows integration of functional modules into nanoparticles as a practical and powerful approach to functionalization of materials. One of the supramolecular host cucurbit[8]uril (CB[8]) with the specific cavity and port dimensions can accommodate two aromatic guests such as viologen and naphthol groups to form stable ternary assemblies driven by host-stabilized charge transfer interactions.[13] Furthermore, the stable ternary structure can be destroyed and spontaneously disassemble after obtaining electrons in a reducing environment.[14] These properties offer the opportunity to construct environmental-sensitive gene carriers.

Herein, the CB[8] based self-assembled supramolecular dendritic nanosystem, (DNCVP (Dendron-Naphthol(DN)/Viologen-PEG(VP)⊂CB[8])) is designed and prepared for gene delivery. In this case, CB[8] is the supramolecular host and the guest consists of two main parts. First, the dendron-naphthol (DN) unit consists of a third-generation dendritic segment coupled terminally with a naphthol moiety and the abundant surface amino groups allow efficient transport of nucleic acids via electrostatic interactions. Second, the viologen-PEG (VP) unit is composed of the violet sperm section linked to PEG via a pH-sensitive hydrazone bond to improve the in vivo stability and biocompatibility of the carrier. The cavity of CB[8] accommodates the DN moiety and VP part to form a stable DNCVP supramolecular delivery vector. The DNCVP/gene complex which is fabricated by electrostatic interaction is able to drop the out layer PEG in an acidic environment to significantly promote cellular internalization by tumor cells, thus achieving tumor-targeted transport of genes.

2. Experimental Section

2.1. Synthesis of DNCVP

2.1.1. Synthesis of the DN Segment

Nitromethane was used to produce 1.2 by the addition reaction in which 1.2 was reduced to 1.3 and then hydrolyzed to 1.4. By multistep amidation, reduction, and hydrolysis, the third-generation dendrimer compound 1.10 was obtained. Thereafter, naphthol reacted in multisteps to produce the intermediate compound 2.2 with a carboxyl group at the end. Finally, intermediate 2.2 reacted with compound 1.10 by amidation to produce 2.3 and the Boc group of compound 2.3 was removed to produce compound 2.4, which is the DN segment. More details are provided in the supplementary materials.

2.1.2. Synthesis of the VP Segment

Bipyridine reacted in two steps to produce compound 3.2 with a carboxyl group at the end. Compound 3.2 reacted with mPEG-ALD by acylation to produce compound 3.3 as the control and compound 3.2 reacted with mPEG-NH_2 by amidation to produce compound 3.3-N. The details are described in the Supporting Information.

2.1.3. Formation of DNCVP Nanocarriers by Self-Assembly of DN, CB[8], and VP

CB[8] (1.0 mmol), VP (1.0 mmol), and DN (1.0 mmol) were weighed and dissolved in water, respectively. The aqueous VP solution was added to the aqueous CB[8] solution dropwise and then the aqueous DN solution was added to the CB[8]/VP complex solution. After 6 h, the solution was dialyzed against water in a dialysis bag (MW = 5,000 Da) and the product DNCVP was obtained after lyophilization (ALPHA 2-4 LSC).

2.2. Self-Assembly of the DNCVP Supramolecular System

2.2.1. Determination of the Stoichiometric Assembly and Binding Constants

To explore the interactions of viologen and naphthol groups with CB[8] during host and guest self-assembly, the chain-like DN-L and VP-L were used to replace the DN segment and VP segment, respectively. The structure was confirmed by ^{1}H NMR. DN-L, VP-L, and CB[8] were dissolved in D_2O in a tube and then sealed for ^{1}H NMR at 22 °C (ADVANCE-DMX500, Bruker, USA). MestReNova was used in the spectrum analysis.

Fourier transform infrared (FTIR) spectroscopy was used to determine the hydrazone bond (Hyd) structure of compound 3.3. Briefly, mPEG-Hyd-OH, compound 3.3, and compound 3.3-N were mixed with potassium bromide, ground, and compressed into tablets prior to FTIR (FITR650, Tianjin, China).

To determine the ratio between the three parts of the self-assembled supramolecular system of DNCVP, Job's experiment was carried out. The total concentration of VP-L and CB[8] was fixed at 5×10^{-5} M first and VP-L and CB[8] solutions with

different molar ratios of 5:0, 4:1, 3:1, 2:1, 1:1, 1:2, 1:3, and 1:4 were prepared. The absorbance at 260 nm was monitored. The difference between the absorbances of the mixed and individual VP-L was recorded as Delta I and the mole fraction of VP-L was plotted against Delta I, which was the Job chart. In the same way, the Job graph of the VP-L/CB[8] solution (1:1) and DN-L solution was obtained as aforementioned at the excitation wavelength of 273 nm, while the total concentration constant was set to 1×10^{-5} M. The change in the fluorescence intensity was plotted to determine the combination ratio of the three.

The binding ratio was obtained depending on the change of absorption peak and absorbance. For convenience, several solutions were prepared. [A solution]: 1.0 mM CB[8] solution; [B solution]: 0.020 mM VP-L solution; [C solution]: 0.10 mM VP-L/CB[8] solution (1:1 mixing); [D solution]: 10 mM DN-L solution. One microliter of the A solution was put in a cuvette and 5, 10, 15, 20, 25, 30, 35, and 40 μL of the B solution were dropped. UV–visible spectrophotometry was conducted before and after titration in the range of 200–1000 nm. Likewise, 1 mL of the C solution was titrated by adding 2, 4, 6, 8, 10, 12, 14, 16, 18, and 20 μL of the D solution UV–Vis was performed at 200–1000 nm. To further verify the binding ratio and obtain the binding constant between the three parts, the reciprocal of the CB[8] concentration was set as the abscissa and $I_0/(I-I_0)$ was plotted on the ordinate, where I referred to the absorbance of the solution and I_0 referred to the absorbance of the titrated solution. The binding constant K was obtained by linear fitting.

2.3. Characterization of the DNCVP Supramolecular System

The size and microscopic morphology of the materials were observed by transmission electron microscopy (TEM). To monitor the impact of PEG strands on the vector stability, the DNCVP vehicle and siRNA were mixed with various N/P (N/P = 5, 10, 20, 30, 40, 50) and then statically incubated for 30 min to form the nanocomplexes. The change in particle size at pH of 7.4 and 6.5 was measured at 0.5, 4, 8, and 24 h by DLS (ZEN360, Malvern, UK), respectively. To validate the ability of the acid response of the vector, the changes in the Zeta potentials were measured before and after the acid treatment. To further verify the reduction response ability of the vehicle, the DNCVP/siRNA complex was treated with the sodium metabisulfite solution. The particle size was measured by DLS.

The stability in serum was examined by the protein absorption assay at different pH values. The four groups were defined as saline (as negative control), DNCV (without PEG), DNCVP(Hyd) (DNCVP containing hydrazone bond), and DNCVP(Ami) (DNCVP containing amide bond). The materials were mixed with the bovine serum albumin (BSA) at pH values of 7.4 and 6.5, respectively. After incubation for 2 h, the supernatant was removed. The total protein content was measured by a BCA protein assay kit and protein adsorption was calculated.

The agarose gel electrophoresis assay was adopted to evaluate the gene loading capacity of DNCVP, DNCVP stimulated by acidic conditions, and DNCVP stimulated under reduction conditions. 1% agarose gel electrophoresis (Basic, Bio-rad, USA) was photographed by a gel image system (Universal Hood II, XRS, USA).

2.4. Cell Culture

The cell culture experiments were performed using HEK293 human-derived kidney embryonic cells and B16F10 mouse-derived melanoma cells. The B16F10 cells were grown in the RPMI-1640 medium and HEK293 in DMEM (Incomplete high glucose, Gbico, USA) supplemented with 10% of FBS (Gbico, USA) and 1% of penicillin–streptomycin (Beyotime, Shanghai, China) at 37 °C in 5% of CO_2. The medium was refreshed every 2 days.

2.4.1. Cell Uptake

The cellular uptake of NP was explored by confocal laser scanning microscopy (CLSM, Olympus, FV1000, JP). Specifically, B16F10 were seeded at a density of 8.0×10^4 cells well^{-1} on 24-well plates containing glass coverslips and grown to 90% confluence after 18 h. The DNCVP solution and 0.3 μg FAM-siRNA (GenePharma, Shanghai, China) were mixed at N/P = 20. The cells were incubated in the mixture with serum-free medium for 2, 4, and 12 h, respectively. Afterward, lysosome dye Lyso-Tracker Red (Beyotime, Shanghai, China) was added and the cells were washed with PBS and fixed with 4% paraformaldehyde. The nuclei were stained with DAPI (Beyotime, Shanghai, China) and photographed by CLSM.

Flow cytometry was employed to determine the uptake efficiency. The B16F10 cells were seeded on glass coverslips and cultured for 18 h. The DNCVP(Hyd) solution and DNCVP (Ami) solution were mixed with 0.3 μg FAM-siRNA at N/P = 20, respectively. The cells were incubated in the mixture with serum-free medium for 2 and 4 h. After incubation, the cells were washed and collected with PBS for flow cytometry (NovoCyte, Agilent, USA) with the aid of the Flowjo software.

2.4.2. Cytotoxicity Assay

The cell cytotoxicity was assessed by the MTT assay (MTT, Energy-chemical, Shanghai). In brief, the B16F10 cells were seeded at a density of 1.5×10^4 cells well^{-1} on 96-well plates and grown to 90% confluence after 18 h. The cells were incubated for different concentration groups of DNCVP, DNCV, and PEI-25 K with serum-free medium and the RPMI-1640 medium was the positive control and sterile water the negative control ($n = 4$). The medium containing MTT (0.5 mg mL^{-1}) was added to each well and co-cultured. After the cells were incubated in darkness for 4 h, DMSO was added to dissolve the crystals. The optical density (OD) of the supernatant at $\lambda = 570$ nm was monitored on the microplate reader (SpectraMax 190, Molecular Devices, USA) and HEK293 was cultured by DMEM medium with the conditions and processes being the same as above.

2.5. In Vitro Gene Delivery

2.5.1. Transfection Efficacy of the Enhanced Green Fluorescent Protein (EGFP)

The efficiency of transfection was monitored using a plasmid with green fluorescent protein expressed in the HEK293 and

B16F10 cells. The DNCVP vector served as the experimental group and the cationic gene vector PEI-25 K as the positive control. The B16F10 cells were seeded at a density of 4.0×10^4 on 24-well plates containing glass slides and grown to 50% confluence after 18 h. Afterward, the DNCVP solution and 1.0 μg of pcDNA-enhanced green fluorescent protein plasmids (PcDNA3.1-EGFP, General Biosystems, USA) were mixed (N/P = 5, 10, 20, and 30, respectively). It was completed with the serum-free RPMI-1640 culture medium, mixed, and added to the well. After culturing for 48 h, the EGFP expressions were observed and photographed by inverted fluorescence microscopy and HEK293 was cultured by the DMEM medium under the same conditions.

2.5.2. Transfection Efficiency of Luciferase

To quantitatively compare the efficiency of vector transfection, the transfection effects of DNCV, DNCVP(Hyd), and DNCVP(Ami) carrying the firefly luciferase plasmid pGL3 (GenePharma, Shanghai, China) for different N/P were investigated. The B16F10 cells were seeded at the density of 1.0×10^4 on 96-well plates and grown to 50% confluence after 18 h. Afterward, the DNCVP, DNCVP (Hyd), DNCVP (Ami) solution, and 0.2 μg pGL3 firefly luciferase plasmid were mixed (N/P = 5, 10, 20, and 30, respectively) and left for 30 min. It was completed with a serum-free RPMI-1640 culture medium, mixed, and added to the well ($n = 3$). After culturing for 48 h, the cells were washed with PBS and lysed with an appropriate amount of RIPA containing 1% PMSF. After the lysates were centrifugated at 10 000 rpm, the supernatant was quantified by BCA Assay (Boster Biological Technology, Wuhan, China). The luciferase reporter gene assays were performed using the Firefly Luciferase Reporter Gene Assay Kit (Beyotime, Shanghai, China) according to the manufacturer's protocol. A fluorometer (FB 12, Nikon Corporation, Japan) was used to calculate the luminous intensity per mg of protein to derive the luciferase expression efficiency of each group. HEK293 was cultured by the DMEM medium under the same conditions.

2.5.3. Gene Silencing Experiment

To investigate the expression of the target protein, western blotting (WB) was performed. After treating with free siGAPDH (CGGGAAGCUCACUGGCAUG, General Biosystems, USA), DNCVP(Hyd)/siGAPDH or DNCVP(Ami)/siGAPDH, the expression of GAPDH was compared to illustrate the silencing efficiency of the vector. The cationic gene vector PEI-25 K was the positive control and the PBS group was the blank control. In detail, the B16F10 cells were seeded at the density of 3.0×10^5 on six-well plates and grown to 50% confluence after 18 h. Each vector solution was mixed with siGAPDH (at a dose of 40 nM, N/P = 20) and the vector-free and gene-free group was replaced by an equal amount of fresh PBS. The complexes were supplemented with the serum-free RPMI-1640 culture medium, mixed, and added to the well ($n = 3$). After culturing for 48 h, the cells were washed with PBS and lysed with an appropriate amount of RIPA containing 1% PMSF. After the lysates were centrifugated at 10 000 rpm, the supernatant was quantified by the BCA Assay. The protein samples were boiled for 10 min and 15 μL of the total protein and buffer were loaded, separated by 10% SDS-PAGE, and transferred onto a polyvinylidene fluoride membrane. The membrane was blocked for 2 h and then the primary anti-β-actin and GAPDH (Boster Biological Technology, Wuhan, China) antibody were incubated overnight at 4 °C. After washing the next day, the membranes were incubated with secondary antibodies for 2 h and observed by the infrared imaging system (CLX-9140, LI-COX, USA).

2.6. Animal Experiments

The animal experiments were authorized by the Institutional Animal Care and Use Committee (IACUC) of Zhejiang University. All the animals were housed and treated in strict accordance with the guidelines of The National Regulation of China for Care and Use of Laboratory Animals. To eliminate stress, the nude mice and C57LB/6 acclimated to the conditions for at least 3 days before the experiments.

2.6.1. In Vivo Distributions

In the subcutaneous tumor xenograft models, the B16F10 cell suspension was injected into the left flank of the nude mice. Tumors with a diameter of larger than 5 mm were available within ≈10 days. To observe the distribution of the nanocomposites in various organs, the mice were randomly divided into four groups and tail-vein injected with Cy5-siRNA (GenePharma, Shanghai, China), DNCVP(Ami)/Cy5-siRNA, DNCVP(Hyd)/Cy5-siRNA, and PEI-25 K/Cy5-siRNA (Cy5-siRNA at a dosage of 1.0 mg kg^{-1}). Fluorescence in vivo was observed and photographed at 1, 6, 12, and 24 h. Subsequently, the mice were euthanized. The heart, liver, spleen, lung, kidney, and tumor were dissected and photographed by the in vivo fluorescence imaging system (MK50101-EX, Cri, USA). Finally, the tissues and tumors were washed, frozen at −80 °C, and cryo-sectioned (HM525, Thmero, Germany). The fluorescence distribution was observed and photographed by inverted fluorescence microscopy (Nion Eclipse, Nikon, Japan).

2.6.2. Luciferase Activity Analysis

In the subcutaneous tumor xenograft models, the B16F10 cell suspension was injected into the left flank of C57LB/6, and tumors with a diameter of larger than 5 mm were observed within ≈10 days. To measure the distribution of the nanocomplexes in various organs and gene expression in the body, the expression of luciferase in vivo was evaluated. The mice were randomly divided into five groups ($n = 3$) and each group was injected with PBS pGL3, DNCVP(Ami)/pGL3, DNCVP(Hyd)/pGL3, and PEI-25K/pGL3 (pGL3 with a dosage of 1.0 mg kg^{-1}). The heart, liver, spleen, lung, kidney, and tumor were dissected and removed after the mice were euthanized at the time point of 48 h. The samples were washed and homogenized with an ultrasonic processor. Afterward, the lysates were centrifugated at 10 000 rpm and the supernatant was quantified by the BCA Assay. The luciferase reporter gene assays were performed using the Firefly Luciferase Reporter Gene Assay Kit according to the manufacturer's protocol. A fluorometer was used to calculate the

luminous intensity per mg of protein to determine the luciferase expression efficiency of each group.

2.7. Statistical Analysis

The tests were done three times and the results were represented as mean ± standard deviation ($n \geq 3$). All the quantitative data were subjected to one-way ANOVA or two-way ANOVA with significant differences calculated. Values of $^{*}p < 0.05$, $^{**}p < 0.01$, and $^{***}p < 0.001$ were considered statistically significant.

3. Results

A DNCVP supramolecular self-assembling gene delivery system that can carry nucleic acid molecules in a stable and effective manner is designed. As depicted in **Scheme 1**, the third-generation dendrimer ends are coupled to the naphthol moieties and the abundant amino groups on the surface absorb nucleic acids effectively through electrostatic interactions, while the violet sperm moieties are coupled to PEG through the pH-sensitive hydrazone bonds. They are accommodated in the cavity of CB[8] to produce a stable supramolecular system by self-assembly. When the DNCVP and gene nanocomplex are formed electrostatically, PEG can avoid to be cleared in blood circulation. Furthermore, the hydrazine bond is broken due to lower pH after reaching the tumor site consequently dropping the PEG layer, exposing positive charges, and being endocytosed by tumor cells. Lysosomal escape is completed by the "proton sponge" effect and finally, the intracellular host–guest structure is disassembled and the genes carried by DNCVP are released to produce the desirable effects.

3.1. Synthesis and Characterization

Synthesis of the DN and VP units is described in Supplementary Information and the structures are verified by ^{1}H NMR (Figure S1–S8, Supporting Information). FITR is employed to analyze the hydrazone structure. As shown in **Figure 1**B, the peaks at 3340 and 3342 cm^{-1} are from the amino group on the hydrazone bond of compound 3.3 and intermediate mPEG-Hyd-OH, respectively, verifying formation of the hydrazone structure of compound 3.3. The amino group absorption peak reflecting the amide bond of compound 3.3-N can be observed at 3293 cm^{-1}.

3.2. Determination of the Stoichiometric Assembly and Binding Constants

The self-assembly process of the three segments of DN, VP, and CB[8] is illustrated in Scheme 1. The viologen group of the guest

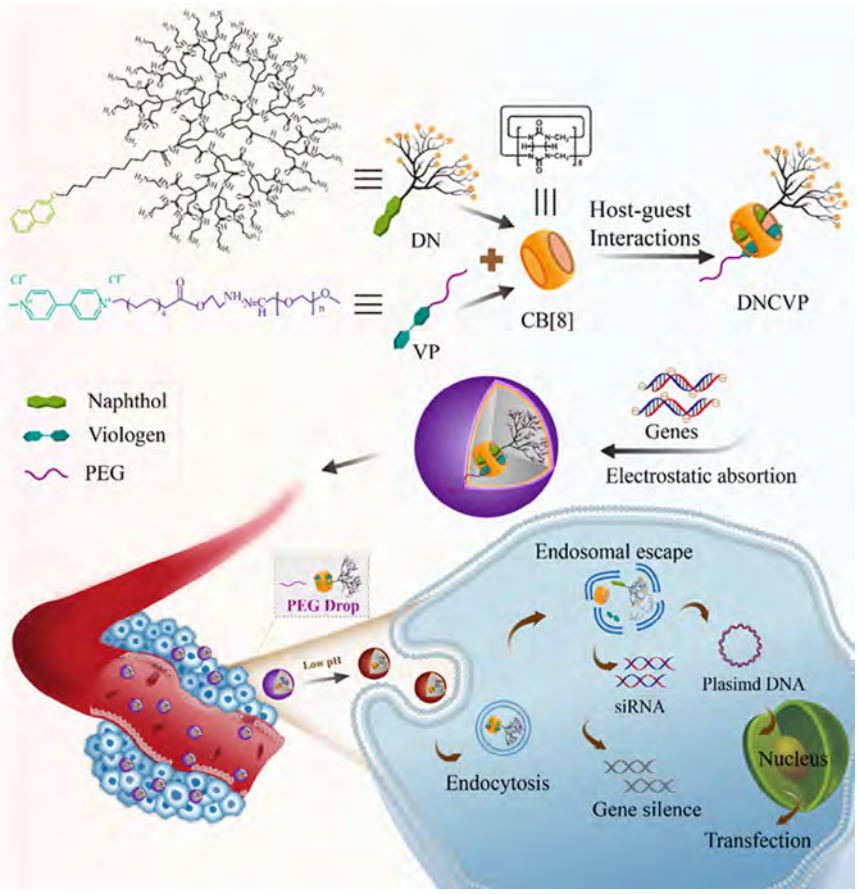

Scheme 1. Fabrication of the self-assembled supramolecular dendrimer and delivery of nucleic acids such as plasmid DNA and siRNA in tumor gene therapy.

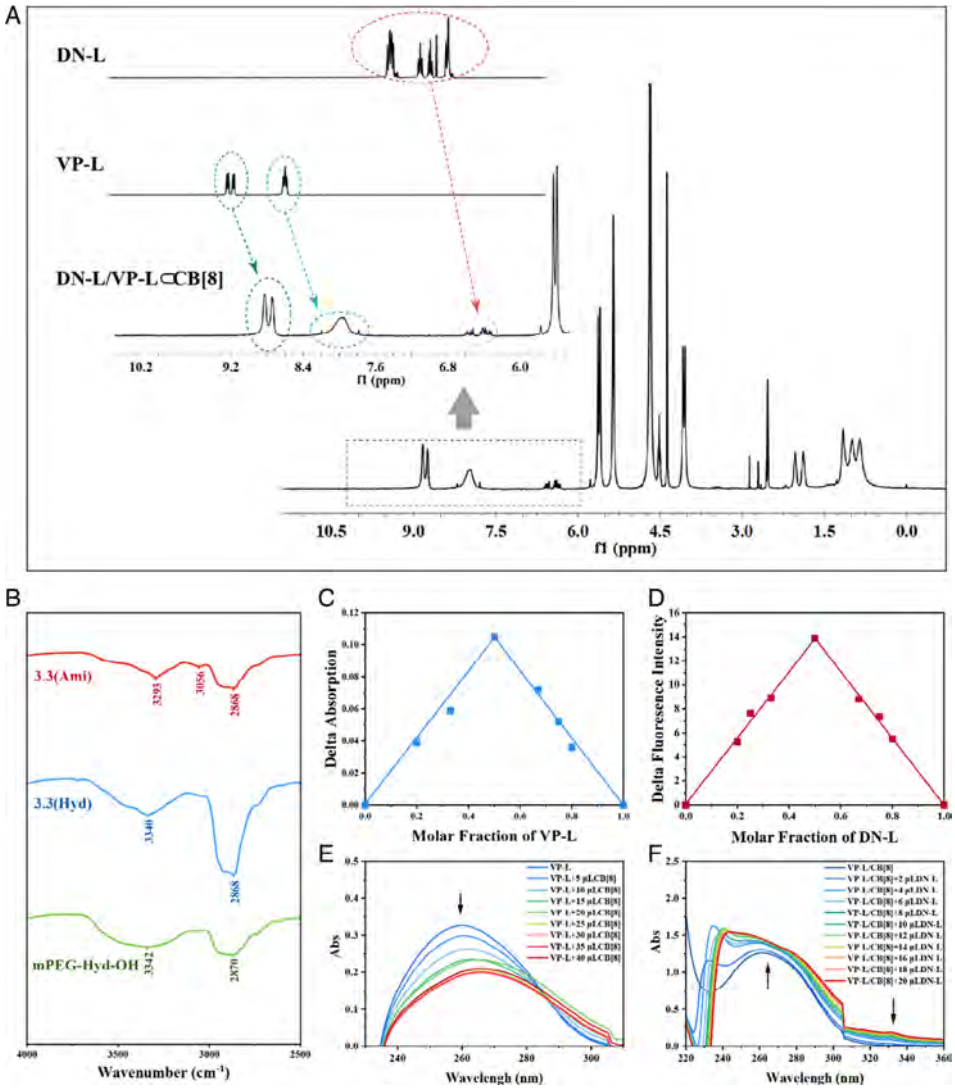

Figure 1. A) ^{1}H NMR spectra of DN-L/VP-L⊂CB[8] and ^{1}H NMR comparison of DN-L, VP-L, and DN-L/VP-L⊂CB[8] (the molar ratio of DN-L, VP-L, and CB[8] was 1:5:1); B) FTIR spectra of 3.3-N, 3.3 and mPEG-Hyd-OH; C) Job's plot of VP-L and CB[8] (total concentration = 5×10^{-5} M); D) Job's plot of DN-L and VP-L/CB[8] (total concentration = 1×10^{-5} M); E) UV–Vis spectra of VP-L solution titrated with CB[8] solution and F) VP-L/CB[8] solution titrated with DN-L solution, respectively.

VP segment first enters the CB[8] host cavity and naphthol of the DN segment enters the cavity as well. They are combined with a certain ratio in self-assembly to produce the supramolecular compound. To determine whether these segments are self-assembled, ^{1}H NMR is performed and the results of DN-L, VP-L, and self-assembled DN-L/VP-L⊂CB[8] are presented in Figure 1A. The characteristic peaks of protons from viologen and naphthol groups in DN-L/VP-L⊂CB[8] shift to a high field. This phenomenon can be explained by the shielding effect upon formation of host–guest complex mainly driven by the charge transfer interactions in the cavity of CB[8].

Self-assembly of DN-L, VP-L, and CB[8] is analyzed further using Job's theory. According to Job's theory, the total concentration of the host and guest is constant and the ratio between the host and guest molecules can be calculated by the difference between the absorption peaks of the solution and a single molecule at a specific wavelength. The self-assembly ratio of CB[8] and VP-L is determined from the spectrum at 260 nm. As shown in Figure 1C, the mole fraction of VP-L in the solution is 0.5, indicating that CB[8] and VP-L are assembled with a ratio of 1:1. Before and after this point, the absorbance changes with the mole fraction of VP-L exhibiting positive and negative linear relationships consistent with Job's theory. The self-assembly ratio of DN-L and VP-L/CB[8] is determined from the fluorescence spectra obtained at a concentration for different molar ratios and the intensity change at the emission wavelength of 355 nm is monitored. Figure 1D shows that the mole fraction of DN-L in the solution is also 0.5, meaning that the DN-L, CB[8], and VP-L self-assembly ratio of the host and guest is 1:1:1.

Self-assembly of the three parts is further investigated by UV titration and the UV-vis results are presented in Figure 1E. The absorbance at 260 nm decreases during titration until the CB[8] and VP-L are equimolar (volume of 20 μL). It can be explained that the viologen group of VP-L enters the cavity of CB[8] through self-assembly and dropping of CB[8] and so the UV absorbance decreases continuously. Afterward, the absorbance exhibits almost no change when CB[8] is added dropwise, indicating that CB[8] can only hold an equimolar amount of VP-L. Therefore, the self-assembly ratio is 1:1. Similarly, there are three main changes as shown in Figure 1F. After introduction of the DN-L solution, a new absorption peak appears at near 333 nm but it is not found from DN-L, VP-L, and VP-L/CB[8], thereby presenting direct evidence of self-assembly during which the electron-rich viologen group and electron-deficient naphthalene phenolic group undergo charge transfer in the cucurbituril cavity.[13a,b,15] In addition, the absorption peak from the naphthol group appears at 230 nm and then a significant red shift occurs during DN-L titration. The absorbance of the viologen peak at 259 nm increases and blue-shifts. The changes stop when the molar amount of DN-L and VP-L/CB[8] in the solution is the same (volume of 10 μL), proving that the cavity of CB[8] is capable of containing an equimolar amount of VP-L and DN-L. Hence, the host–guest self-assembly occurs with a ratio of 1:1:1 of the three segments.

The Hildebrand–Benes equation (Equation (1)) can be used to derive the assembly ratio of each segment. In the equation, a and b are constants, I is the absorbance of the mixed solution, and I_0 is the absorbance of the titrated solution. The reciprocal [B] is a function of the $I_0/(I-I_0)$

$$\frac{I_0-1}{I_0}=\frac{a}{b-a}\left(\frac{1}{K}[B]^{-1}+1\right) \quad (1)$$

A linear relationship indicates that the ratio is 1:1. In this case, the linear equation of $Y=A+B\cdot X$ is obtained by fitting (A/B is the binding constant K) and the results based on UV titration are plotted (Figure S9, Supporting Information). Regardless of whether the CB[8] solution is used to titrate the VP-L solution or DN-L solution to titrate VP-L/CB[8], the fitted curves of $I_0/(I-I_0)$ to $1/[B]$ exhibit good linearity, revealing that the ratio is 1:1:1. The binding constants K of step titration are 7.71×10^3 and 4.04×10^3, respectively.

3.3. Characterization of the DNCVP Supramolecular System

The morphology and structure of each complex treated with different conditions are examined by TEM. As shown in **Figure 2**A, DNCVP/siRNA has a spherical and uniform morphology with a diameter of about 200 nm, which is also confirmed by the DLS data. Figure 2B shows the DNCVP/siRNA nanocomplex maintains the spherical shape at a pH of 6.5. Although the outer PEG may be lost by breaking the hydrazone bond in an acidic environment, the positively charged surface can still condense the genes by electrostatic interaction. As shown in Figure 2C, the structure of the DNCVP/siRNA nanocomplex treated with a reducing $Na_2S_2O_5$ solution changes considerably. The stability of the nanocomplex is disrupted by disassembly of the supramolecular system and as a result, the morphology becomes fuzzy, disordered, and irregular.

The size and zeta potentials of the DNCVP/siRNA nanocomplex before and after stimulation with different N/P, pH, and reduction conditions are determined. Comparing Figure 2D with Figure 2E, the size of the nanocomposite does not change a lot in the PBS solution at the pH of 7.4 and remains below 300 nm within 8 h, which is easy to be endocytosed by cells. On the contrary, with extended incubation time at the pH of 6.5 in PBS, the particle size increases rapidly reaching 500 and 800 nm after 8 and 24 h, respectively. It can be explained that when the hydrazone bond breaks and the PEG falls off under the acidic condition of pH of 6.5, the stability of the nanocomplex is affected and larger particles are observed with time, indicating that the PEG layer wrapped on the surface can maintain the stability before reaching the acidic environment of tumors.

Figure 2F shows that the Zeta potentials are below 10 mV for N/P ratios ranging from 5 to 50 at the pH of 7.4. In comparison, the Zeta potential of nanocomplex reaches 35 mV at the pH of 6.5, suggesting that the positive charge of the dendrimer is exposed after cleavage of the hydrazone bond under the acidic condition. The particle size distribution of the DNCVP/siRNA without and with reduction stimulation is shown in Figure S10, Supporting Information. The average hydrodynamic sizes are 267.7 and 397.3 nm, respectively, disclosing that the structure of DNCVP/siRNA changes under reduction conditions. The serum stability is expressed by measuring the protein adsorption rates in the bovine serum protein solution. As shown in Figure S11, Supporting Information, the non-PEG-modified DNCV exhibits the highest protein adsorption rate due to the reaction between negatively charged bovine serum proteins and positively charged amino groups. The protein adsorption rate of DNCVP (Ami) remains low at pH of 7.4 and 6.5. In contrast, the protein adsorption rate of DNCVP(Hyd) increases from 7% to 27% after incubation for 2 h in PBS at the pH of 6.5, showing a significant difference due to increased protein adsorption from breakage of the hydrazone bond in the acidic environment. Exposure to more positive charges after PEG shedding enhances protein adsorption. These results suggest that the PEG-modified nanoparticles reduce protein adsorption, improve serum stability, and produce acidic response of DNCVP carriers.

The gene binding ability is determined by agarose gel electrophoresis. Figure 2G–I shows the blocking results of DNA and siRNA condensed by DNCVP, acid-treated DNCVP, and reductive $Na_2S_2O_5$ solution-treated DNCVP. The DNCVP condenses both DNA and siRNA at small N/P ratios and has good gene-binding ability. The N/P ratios decrease when DNCVP is treated in an acidic medium (PBS, pH = 6.5), revealing that the pH-sensitive hydrazone bond is broken, abundant amino groups are exposed on the surface, and the acid-treated DNCVP can bind negatively charged genes better. Afterward, the binding N/P ratios become larger when DNCVP is under the reduction condition ($Na_2S_2O_5$), suggesting disassembly of DNCVP in the reduction environment.

3.4. Cell Biocompatibility

The MTT method is a common way to assess cytotoxicity. **Figure 3**A,B show the cell survival rates of HEK293 and B16F10, respectively, after incubation with DNCVP, PEG-free

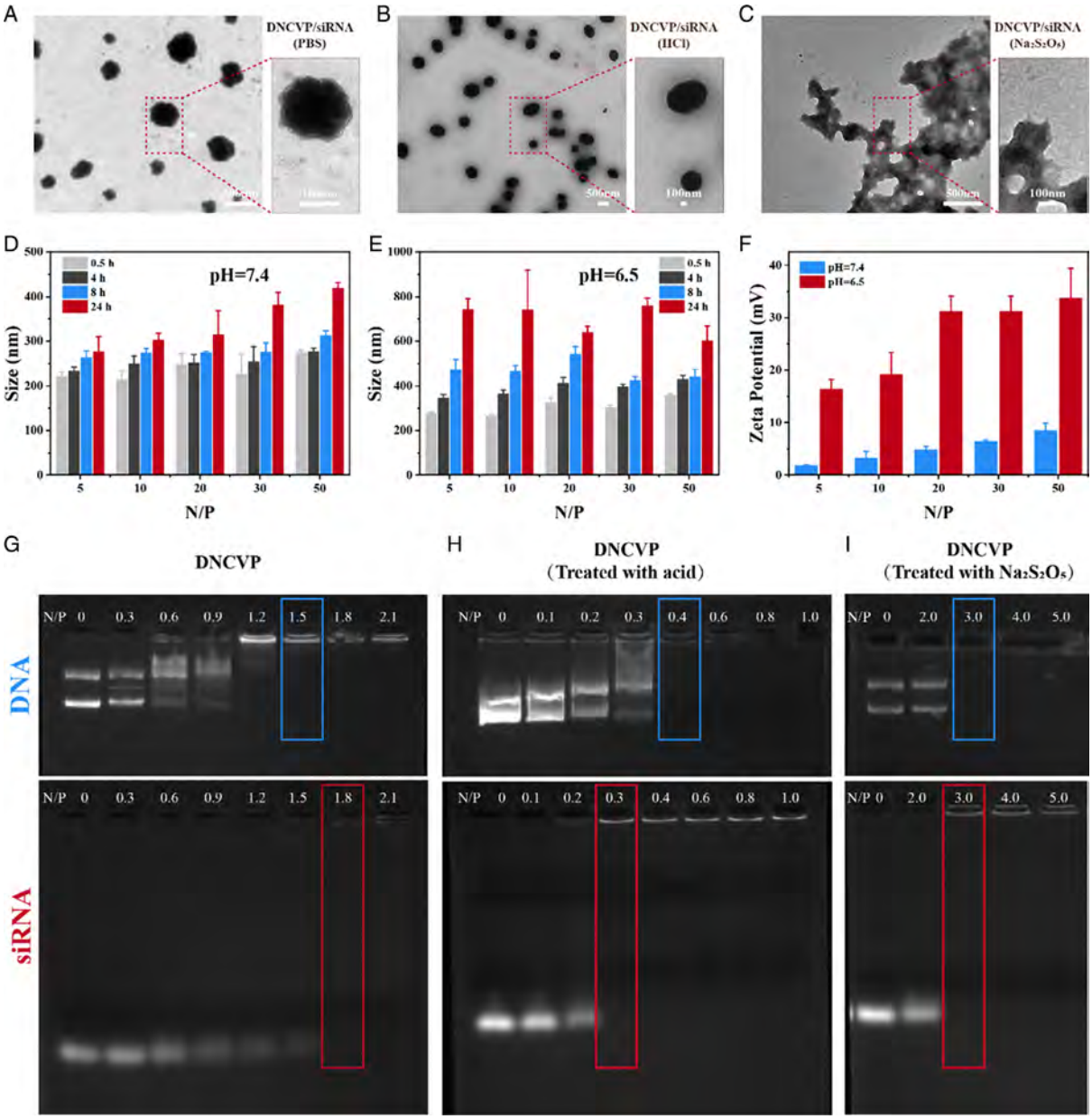

Figure 2. TEM images of A) DNCVP/siRNA at pH of 7.4 and N/P of 20, B) DNCVP/siRNA at pH 6.5, and C) DNCVP/siRNA treated with $Na_2S_2O_5$; particle size of DNCVP/siRNA with different N/P incubated in D) pH = 7.4 and E) pH = 6.5 PBS for different time; F) Zeta potentials at different pH; Agarose gel retardation of plasmid DNA and siRNA condensed by G) DNCVP, H) DNCVP treated with acidic PBS, and I) DNCVP treated with $Na_2S_2O_5$.

DNCVP (DNCV), and positive control PEI-25K for 4 h with the N/P ratio of 4. DNCVP and DNCV display lower cytotoxicity than PEI-25K and the cytotoxicity of PEG-modified (DNCVP) is lower than that of the PEG-free one (DNCV), proving that the outer PEG reduces the toxicity and improves the biocompatibility. In addition, the cell survival rate of the DNCVP is larger than 90% at the transfection dose ensuring low biological toxicity of the carrier.

In addition to cytotoxicity, cellular uptake efficiency is an important factor in gene delivery. The nanodelivery system is generally taken up by endocytosis and so flow cytometry is employed to study the uptake behavior of the vector system by the cells. As shown in Figure 3C, the FAM-siRNA uptake efficiency of the B16F10 cells is quantitatively determined by flow cytometry after incubation for 2 and 4 h with free FAM-siRNA, DNCVP(Hyd)/FAM-siRNA. and DNCVP(Ami)/FAM-siRNA nanoparticles. The free FAM-siRNA group shows negligible green fluorescence since free siRNA is unstable and negatively charged, while more than 20% of the cells show green fluorescence after incubation for 2 h, implying that both DNCVP (Hyd) and DNCVP (Ami) can protect siRNA from degradation and are transported into the cells. The cellular uptake efficiency which is time-dependent reaches almost 50% after 4 h.

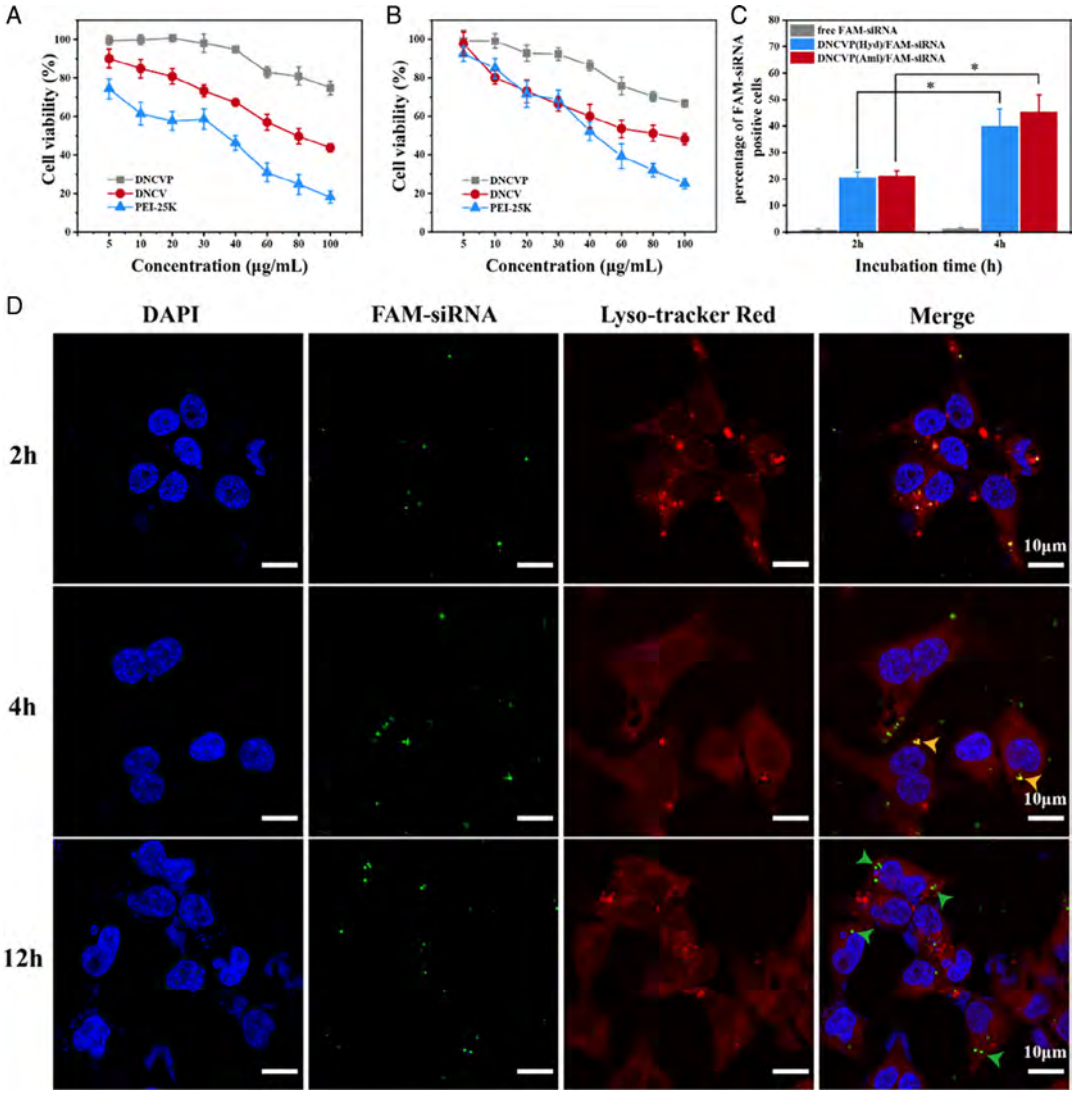

Figure 3. Cell viability of A) HEK293 and B) B16F10 treated with DNCVP, DNCV, and PEI-25 K ($n = 4$); C) cellular uptake efficiency of B16F10 treated with free FAM-siRNA, DNCVP(Hyd)/FAM-siRNA, and DNCVP(Ami)/FAM-siRNA for 2 and 4 h determined by flow cytometry ($n = 3$, $^*p < 0.05$); D) fluorescent confocal microscopy images of B16F10 treated with DNCVP/FAM-siRNA for 2, 4, and 12 h (scale bars = 10 μm).

The cellular uptake behavior is evaluated by CLSM and Figure 3D shows the cellular uptake of DNCVP/FAM-siRNA nanoparticles in the B16F10 cells. Here, the lysosome is labeled by Lyso-Tracker Red (red), FAM-siRNA shows green fluorescence, and the nuclei are stained by DAPI (blue). Similar to the flow cytometry results, green fluorescence appears at 2 h and becomes stronger at 4 h, indicating improved intracellular uptake with time. The red and green fluorescence partially overlaps (yellow arrow) indicating that the nanocomplexes are incorporated into the lysosomes. There is almost no overlapping yellow fluorescence at 12 h but some green fluorescence is observed (green arrow). Meanwhile, the uptake of free RNA is carried out as the negative control in Figure S12, Supporting Information. In contrast to DNCVP/siRNA, the green fluorescence of free FAM-siRNA is very weak. It diffuses in the cells and becomes weak at 12 h. These results indicate that the DNCVP can protect siRNA from degradation and enhance the cellular uptake of siRNA, which is crucial to intracellular transportation of genes.

3.5. In Vitro Gene Delivery

The expression of EGFP is used to identify the efficiency of transfection. **Figure 4**A shows the in vitro transfection images of DNCVP/pEGFP in the B16F10 and HEK293 cells with different N/P ratios by inverted fluorescence microscopy, and PEI-25K was used as a positive control in its optimal N/P ratio at the same time. According to the images, the transfection efficiency is N/P dependent. It becomes higher when the N/P increases. However, when the N/P reaches 30, the transfection efficiency decreases. The explanation is probably that the increased cationic material makes pEGFP difficult to release from the nanocomplex. The

strongest fluorescent signal is observed in the DNCVP/pEGFP at N/P = 20 (Figure S13, Supporting Information), which is similar to the positive control PEI-25K/pEGFP. Therefore, N/P = 20 is used for gene transfection or silencing in subsequent experiments. Luciferase transfection can quantitatively measure the transfection efficiency and Figure 4B,C shows the in vitro luciferase transfection efficiency of DNCVP(Hyd)/pGL3, DNCV/pGL3, and DNCVP(Ami)/pGL3 nanocomplexes in the HEK293 and B16F10 cells for different N/P ratios, respectively. DNCV without PEG modification shows a higher transfection efficiency at a smaller N/P ratio due to the exposed positive charge on the vector. DNCVP(Hyd)/pGL3 displays the highest transfection efficiency at the N/P ratio of 20 consistent with previous results on EGFP transfection. In addition, for N/P ratio = 20, the transfection efficiency of DNCVP(Hyd)/pGL3 is significantly higher than that of DNCVP(Ami)/pGL3, probably attributable to the pH-sensitive hydrazone bond that can be cleaved in the acidic lysosome environment for better gene release.

In addition to gene transfection, the gene silencing capability of the DNCVP/siRNA nanocomplex is studied by the WB analysis of the HEK293 and B16F10 cells with the N/P ratio of 20. Figure 4D presents the WB results of PBS, siGAPDH, DNCVP(Hyd)/siGAPDH, DNCVP(Ami)/siGAPDH, and PEI-25K/siGAPDH. DNCVP(Hyd)/siGAPDH, DNCVP(Ami)/siGAPDH, and PEI-25K/siGAPDH exhibit significant protein silencing effects in both B16F10 and HEK293 cells (Figure 4E,F). Among them, the silencing efficiency of DNCVP(Hyd)/siGAPDH group with a hydrazone bond is more than 60%, that is 14% higher than the "golden standard" PEI-25K in HEK293 cells, revealing the excellent gene delivery capability. In contrast, the silencing efficiency of the DNCVP(Ami)/siGAPDH group is slightly weaker. The trend is the same in the B16F10 cells as displayed in Figure 4E, further verifying the good siRNA delivery ability of the DNCVP system.

3.6. In Vivo Gene Delivery

In the in vivo study, Cy5-siRNA is applied to evaluate the distribution of the DNCVP nanocomplex in nude mice monitored by the in vivo optical imaging system. **Figure 5**A,B show the results of in vivo fluorescence imaging. DNCVP/Cy5-siRNA

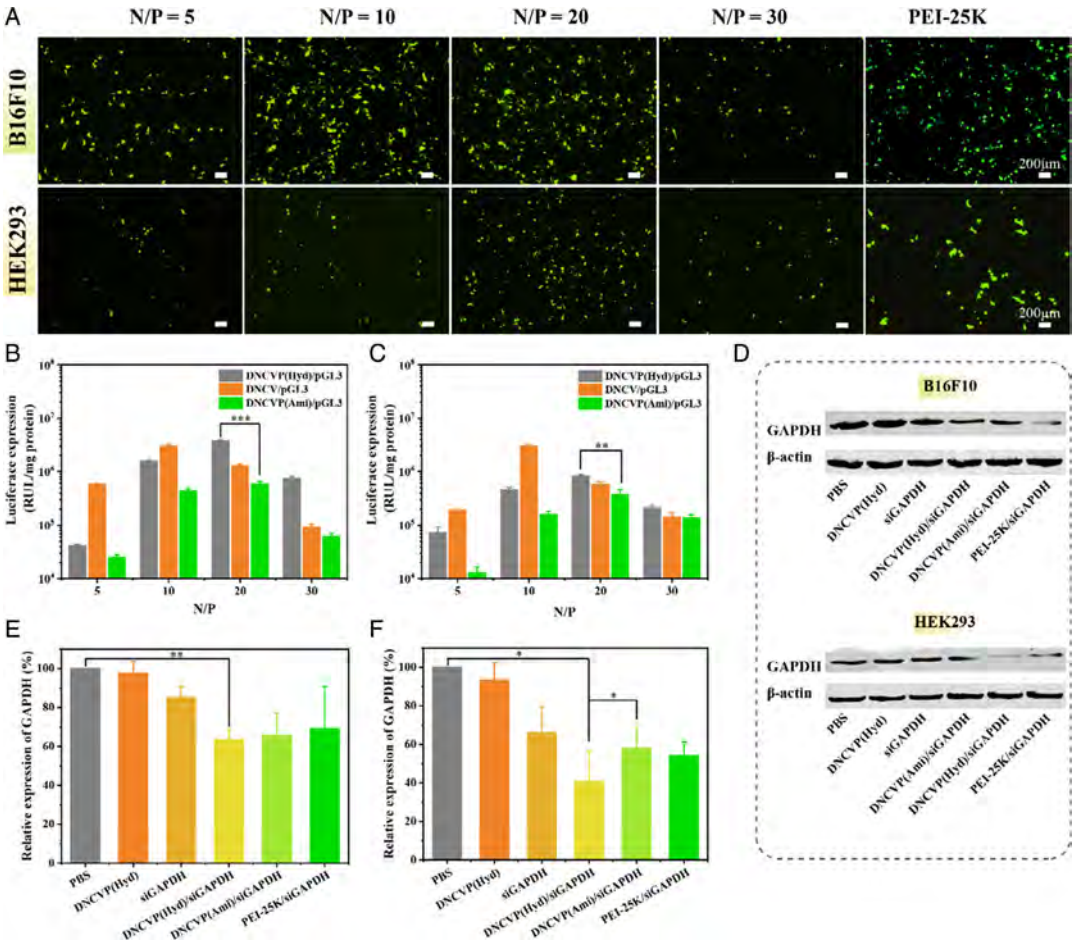

Figure 4. A) In vitro transfection of B16F10 and HEK293 cells treated with DNCVP/pEGFP for different N/P and PEI-25K/pEGFP at N/P = 10 (scale bars = 200 μm); B) HEK293 and C) B16F10 cells treated by DNCVP(Hyd)/pGL3, DNCV/pGL3 and DNCVP(Ami)/pGL3 at different N/P ($n = 3$, $^{**}p < 0.01$, $^{***}p < 0.001$); D) Expression of GAPDH in HEK293 and B16F10 determined by Western Blotting; Silencing efficiency of GAPDH in E) B16F10 and F) HEK293 determined from the light intensities ($n = 3$, $^{*}p < 0.05$, $^{**}p < 0.01$).

accumulates at the tumor site 12 h after injection. The DNCVP (Hyd) group shows better tumor targeting effects than DNCVP (Ami) benefiting from the pH-sensitive structure which can take off the surface PEG in the tumor microenvironment. At 24 h after injection, the DNCVP (Hyd)/Cy5-siRNA can still be found from the tumor site by in vivo fluorescence imaging. The nude mice are sacrificed and the main organs and tumor are excised for fluorescence imaging after 24 h. The tumor of the free Cy5-siRNA group displays negligible fluorescence, whereas the kidney shows very strong fluorescence due to rapid renal clearance of siRNA without the protection of the vector. DNCVP(Ami)/Cy5-siRNA, DNCVP(Hyd)/Cy5-siRNA, and PEI-25K/Cy5-siRNA all exhibit tumor aggregation. In contrast, DNCVP(Hyd)/Cy5-siRNA shows the strongest fluorescence, prolonged circulation time of siRNA, and better tumor targeting. Therefore, DNCVP containing the hydrazone bond is internalized by cells readily due to pH-responsive removal of PEG in the tumor microenvironment. The cryosections of the kidney and tumor tissues are observed and as expected (Figure S14, Supporting Information), the fluorescence images are consistent with the distributions. No fluorescence is observed from the free Cy5-siRNA group, whereas DNCVP(Ami)/Cy5-siRNA, DNCVP(Hyd)/Cy5-siRNA, and PEI-25K/Cy5-siRNA display red fluorescence from the tumor sites. The kidney tissue treated with free Cy5-siRNA exhibits red fluorescence in accordance with Figure 5B.

Since the tumor targeting ability is verified, a B16F10 tumor-bearing mice model is established and pGL3 is employed to confirm the transfection efficiency of DNCVP in vivo. As demonstrated in Figure 5C, the luciferase expression in the heart, liver, spleen, lung, kidney, and tumor sites are detected after transfection. The results of luciferase expression in different organs at 24 h are shown in Figure 5D. In comparison with DNCVP (Ami)/pGL3 and PEI-25 K/pGL3, stronger expression of luciferase is detected from DNCVP(Hyd)/pGL3 corresponding to

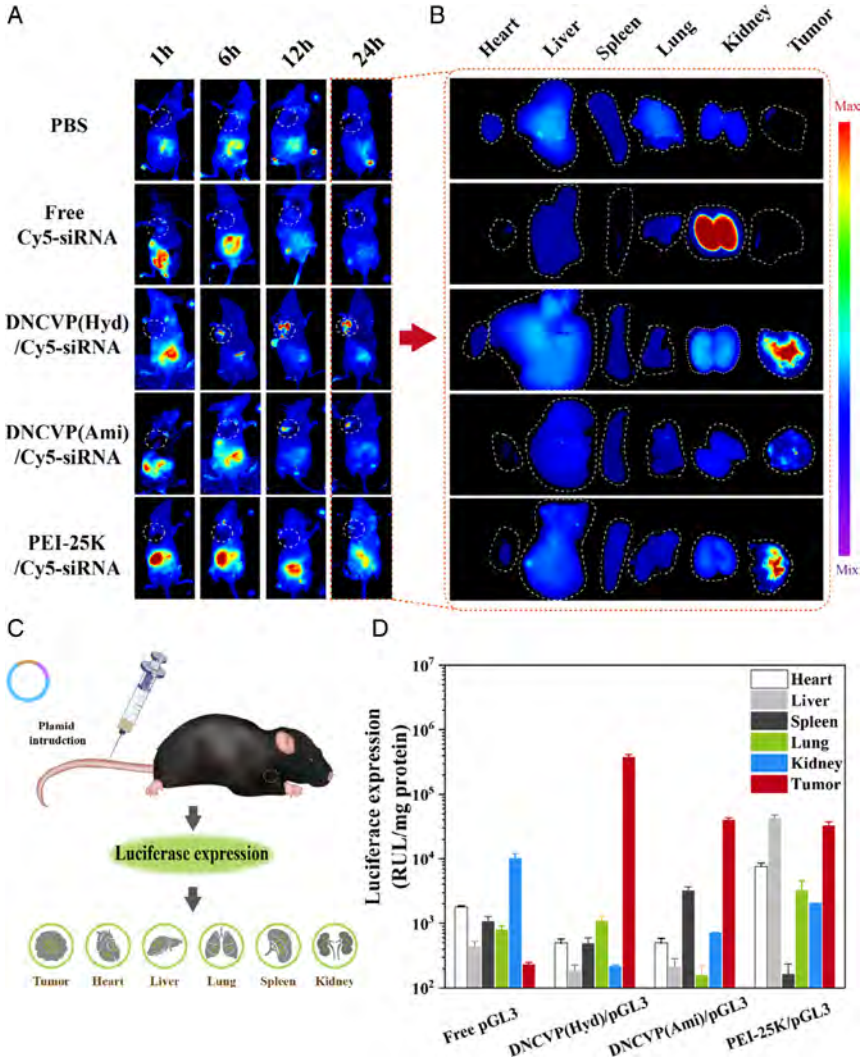

Figure 5. A) Fluorescence images taken at different times and B) fluorescence images taken from various organs and tumor sites 24 h after injection of free Cy5-siRNA, DNCVP(Hyd)/Cy5-siRNA, DNCVP(Ami)/Cy5-siRNA, and PEI-25K/Cy5-siRNA via the tail vein. The tumor area is circled by a dotted line in (A). C) Fluorescence expression in vivo depicted in the schematic diagram of the mouse. D) Luciferase transfection in various organs and tumor sites of C57BL/6 after tail vein injection of free pGL3, DNCVP(Hyd)/pGL3, DNCVP(Ami)/pGL3, and PEI-25K/pGL3 ($n = 3$).

9.5 and 11.6 times increase, respectively. The expression of luciferase in the liver in PEI-25K/pGL3 is 100–200 folds higher than that of other groups, but also 4–15 times higher than that in other organs, indicating that the cationic gene vector PEI-25K may have potential hepatotoxicity, while the DNCVP is more biocompatible. In contrast, transfection of free pGL3 in the kidney is higher than in other organs at 24 h providing evidence that free siRNA is rapidly metabolized and excreted by the kidney. All in all, the in vivo luciferase expression results demonstrate low toxicity, the ability of tumor targeting, and high transfection efficiency of DNCVP.

4. Discussion

Dendrimers are interesting in cancer therapy due to their unique characteristics. Benefiting from the highly branched structure, diverse compounds such as therapeutic drugs, bioactive ligands, targeting molecules, and functional polymers can be conjugated to the surface of the dendrimer in a multivalent fashion. The hydrophobic cavities and charged groups are also able to encapsulate or bind antitumor drugs and genes.[16] Owing to their multifunctional ability, dendrimers have been widely engineered as gene vectors for cancer gene therapy. For example, polyamide-amine (PAMAM) dendrimers are widely used in gene delivery. The gene delivery ability depends on the generation of PAMAM since high-generation PAMAM (G4 or above) has a relatively large molecular dimension and contains sufficient positive charge to condense genes. Nonetheless, the regular dendritic structure becomes an obstacle in the synthesis of high-generation dendrimers.[17] Hence, supramolecular chemistry is implemented in the host–guest self-assembly instead of covalent linkage to simplify the preparation as well as achieve multifunctional modification.

In this work, a supramolecular dendritic gene vector, named DNCVP, is established via self-assembly of amino dendron conjugated naphthol, viologen containing pH-sensitive hydrazone bond linked PEG, and CB[8]. The DNCVP gene delivery system is supposed to condense the genes, take off surface PEG in the acidic tumor microenvironment, undergo endocytosis by cancer cells via endocytosis, escape the lysosome, disassemble under reduction conditions, and then release the genes. To achieve the series of processes and deliver the genes to tumor cells, the DNCVP is synthesized. After confirming the structures of the different parts of the supramolecular by ^{1}H NMR and FTIR, the self-assembly behavior of these three segments is evaluated by ^{1}H NMR, UV titration, and fluorescence titration. CB[8] is able to simultaneously encapsulate two specific guest molecules via noncovalent interactions to form a stable ternary host–guest supramolecule.[18] As expected, ^{1}H NMR demonstrates that the host CB[8] interacts with the two guests, naphthol as well as viologen. The UV and fluorescence data are analyzed according to Job's theory revealing a self-assembly ratio of 1:1:1. The changes in the UV spectra provide experimental evidence of charge transfer between the electron-rich viologen group and electron-deficient naphthalene phenolic group in the CB[8] cavity. The binding constants are calculated to be 7.71×10^3 and 4.04×10^3 by Hildebrand–Benes equation. The results indicate that the DN and VP segments of DNCVP are successfully synthesized and the host CB[8] is capable of self-assembling with the two guests with a molar ratio of 1:1:1 to form the stable DNCVP dendritic gene vector.

As cationic polymeric materials are explored for gene delivery applications, some drawbacks have been discovered. Positively charged dendrimers have restricted usage because they interact with cell membranes and induce cell lysis.[19] To overcome this limitation, PEGylation is a good strategy for structure modification. The surface PEG not only shields the positive charge, disguises the flaws, and increases the appropriateness of cationic dendrimers for gene delivery,[20] but also reduces the undesirable biological recognition by the reticuloendothelial system (RES) and prolongs the blood circulation time of nanomaterials.[21] For instance, Pego et al. have constructed a fully biodegradable PEG-dendritic nanodelivery system by inducing tunable ester bonds which can carry and protect siRNA for cell internalization to achieve intracellular release and transfection of nucleic acid.[22] However, PEGylation is a double-edged sword in surface modification. It has been reported that excessive PEGylation on the nanomaterials decreases cellular uptake and interactions with proteins at the desired sites.[21] As a consequence, we employ the PEG segment containing a pH-sensitive hydrazone bond so that the PEG can be shredded when the nanocomplexes reach the tumor site. The morphology, size, Zeta potential, and gene binding ability of the nanocomplex are analyzed. The surface of the DNCVP complex displays a certain low positive charge after PEGylation. Different conditions are adopted in the experiments to prove whether DNCVP is stimuli-responsive and the results suggest that the positively charged DNCVP is capable of condensing negative genes, removing surface PEG under the acidic condition (pH = 6.5), as well as disassembling under the reduction condition (in $Na_2S_2O_5$). In addition, the protein absorption assay illustrates that DNCVP is stable under normal physiological conditions and has good bioavailability. However, the absorption rate increases due to the drop of surface PEG in the solution at a pH of 6.5. Owning to the good gene binding capacity and stimuli-responsibility, DNCVP is further studied in vitro and in vivo.

The cytotoxicity and transfection efficiency in HEK293 and B16F10 cells are firstly compared to that of PEI-25 K because PEI-25K has been a benchmark of cationic nonviral gene vectors since it was first used in 1995.[23] The cytotoxicity of DNCVP is significantly lower than that of both DNCV (the material without PEG conjugation) and PEI-25K, indicating that the surface PEG successfully lowers the toxicity of cationic materials and DNCVP has good biocompatibility. Similar to other cationic vectors, DNCVP enters the cells via endocytosis. The gene transfection and gene silencing efficiency are monitored using pEGFP, pGL3, and siGAPDH. The green fluorescence and luciferase transfection reveal that DNCVP has excellent transfection efficiency and the optimal N/P ratio for transfection should be 20:1. In addition, the importance of the hydrazone bond in DNCVP is revealed using DNCVP with an amino bond (marked as DNCVP(Ami)). In comparison with DNCVP(Ami), DNCVP(Hyd) achieves significantly higher efficiency in not only transfection of pGL3 but also silencing of siGAPDH. Hence, the in vitro studies disclose satisfactory gene delivery effects of the hydrazone bond containing DNCVP and large potential in in vivo administration.

In vivo studies are conducted via tail vein injection into B16F10 tumor-bearing mice. The biodistribution images illustrate that DNCVP with the hydrazone bond has the best tumor accumulation compared with DNCVP(Ami) and PEI-25K, as manifested by prolonged circulation time of siRNA and improved tumor targeting. Luciferase transfection provides evidence that DNCVP can deliver genes to the tumor site and consequently, DNCVP is a useful gene vector to deliver functional genes in tumor-targeting gene therapy.

Looking forward, this supramolecular system is able to be extended to other applications of biomedicine since versatile segments can be added for different purposes. For instance, we can employ a probe-containing segment to form a theranosis nanoplatform, a peptide-containing segment to get a dual targeting nanoplatform, and so on. This supramolecular self-assembled dendrimer offers an effective strategy to simplify the preparation of dendritic materials and it is an easy way to integrate different segments into a multifunctional dendritic nanoplatform.

5. Conclusion

A supramolecular dendritic gene vector DNCVP is designed using the amino dendron conjugated naphthol, viologen containing pH-sensitive hydrazone bond linked PEG, and CB[8] as building blocks. The dendron segments of DNCVP are synthesized and mixed with CB[8] and self-assembly of the three parts is performed with a molar ratio of 1:1:1. PEG on the surface drops from DNCVP under acidic conditions due to linkage of the pH-sensitive hydrazone bond and DNCVP disassembles under reduction conditions to exhibit the stimuli-responsibility in targeted delivery of genes. The MTT assay illustrates low cytotoxicity due to protection of PEG and in vitro transfection of pEGFP and pGL3 and silencing of siGAPDH further verify the excellent gene delivery effects of DNCVP. In vivo studies demonstrate that the pH-responsive DNCVP promotes tumor accumulation of the nanocomplex and improves the transfection efficiency at the tumor site. This novel supramolecular dendritic gene vector suitable for tumor targeting therapy provides the possibility of easy integration of versatile functional segments, showing promising potential in gene therapy.

Supporting Information

Supporting Information is available from the Wiley Online Library or from the author.

Acknowledgements

X.O. and D.G. contributed equally to this work. This work was supported by the National Natural Science Foundation of China (Grant No. 51603184, 22175107), Zhejiang Provincial Natural Science Foundation of China (Grant No. LY21E030002, LY22H020003), Hangzhou Science and Technology Bureau of China (Grant No. 202203B27), Scientific Research Foundation of Zhejiang University City College (J-202104), City University of Hong Kong Donation Research Grant (DON-RMG 9229021), City University of Hong Kong Strategic Research Grant (SRG 7005505), City University of Hong Kong Donation Grant (9220061), Hong Kong PDFS - RGC Postdoctoral Fellowship Scheme (PDFS2122-1S08 and CityU 9061014), and Hong Kong HMRF (Health and Medical Research Fund) (2120972 and CityU 9211320).

Conflict of Interest

The authors declare no conflict of interest.

Data Availability Statement

The data that support the findings of this study are available from the corresponding author upon reasonable request.

Keywords

dendrimer, gene delivery, host−guest system, supramolecule, tumor targeting

Received: December 9, 2022
Revised: March 3, 2023
Published online: May 1, 2023

[1] a) C. E. Dunbar, K. A. High, J. K. Joung, D. B. Kohn, K. Ozawa, M. Sadelain, *Science* **2018**, *359*, eaan4672; b) C. C. Ma, Z. L. Wang, T. Xu, Z. Y. He, Y. Q. Wei, *Biotechnol. Adv.* **2020**, *40*, 107502.

[2] a) H. Yin, R. L. Kanasty, A. A. Eltoukhy, A. J. Vegas, J. R. Dorkin, D. G. Anderson, *Nat. Rev. Genet.* **2014**, *15*, 541; b) R. Mohammadinejad, A. Dehshahri, V. Sagar Madamsetty, M. Zahmatkeshan, S. Tavakol, P. Makvandi, D. Khorsandi, A. Pardakhty, M. Ashrafizadeh, E. Ghasemipour Afshar, A. Zarrabi, *J. Control. Release* **2020**, *325*, 249.

[3] a) E. Abbasi, S. F. Aval, A. Akbarzadeh, M. Milani, H. T. Nasrabadi, S. W. Joo, Y. Hanifehpour, K. Nejati-Koshki, R. Pashaei-Asl, *Nanoscale Res. Lett.* **2014**, *9*, 247; b) M. Arseneault, C. Wafer, J. F. Morin, *Molecules* **2015**, *20*, 9263.

[4] a) J. Yang, Q. Zhang, H. Chang, Y. Cheng, *Chem. Rev.* **2015**, *115*, 5274; b) M. Ghaffari, G. Dehghan, F. Abedi-Gaballu, S. Kashanian, B. Baradaran, J. Ezzati Nazhad Dolatabadi, D. Losic, *Eur. J. Pharm. Sci.* **2018**, *122*, 311.

[5] a) C. Dufes, I. F. Uchegbu, A. G. Schatzlein, *Adv. Drug Delivery Rev.* **2005**, *57*, 2177; b) P. Kesharwani, K. Jain, N. K. Jain, *Prog. Polym. Sci.* **2014**, *39*, 268; c) P. Kesharwani, A. K. Iyer, *Drug Discovery Today* **2015**, *20*, 536; d) L. Palmerston Mendes, J. Pan, V. P. Torchilin, *Molecules* **2017**, *22*, 1401; e) H. Li, J. Sun, H. Zhu, H. Wu, H. Zhang, Z. Gu, K. Luo, *Wiley Interdiscip. Rev. Nanomed. Nanobiotechnol.* **2021**, *13*, e1670.

[6] a) K. Madaan, S. Kumar, N. Poonia, V. Lather, D. Pandita, *J. Pharm. Bioallied Sci.* **2014**, *6*, 139; b) A. Janaszewska, J. Lazniewska, P. Trzepinski, M. Marcinkowska, B. Klajnert-Maculewicz, *Biomolecules* **2019**, *9*, 330.

[7] a) S. Mura, J. Nicolas, P. Couvreur, *Nat. Mater.* **2013**, *12*, 991; b) T. Ramasamy, H. B. Ruttala, B. Gupta, B. K. Poudel, H. G. Choi, C. S. Yong, J. O. Kim, *J. Control. Release* **2017**, *258*, 226; c) Z. Li, H. Cai, Z. Li, L. Ren, X. Ma, H. Zhu, Q. Zhang, Z. Gu, K. Luo, *Bioact. Mater.* **2022**, *13*, 299.

[8] a) M. Karimi, A. Ghasemi, P. Sahandi Zangabad, R. Rahighi, S. M. Moosavi Basri, H. Mirshekari, M. Amiri, Z. Shafaei Pishabad, A. Aslani, M. Bozorgomid, D. Ghosh, A. Beyzavi, A. Vaseghi, A. R. Aref, L. Haghani, S. Bahrami, M. R. Hamblin, *Chem. Soc. Rev.* **2016**, *45*, 1457; b) S. Ahmadi, N. Rabiee,

M. Bagherzadeh, F. Elmi, Y. Fatahi, F. Farjadian, N. Baheiraei, B. Nasseri, M. Rabiee, N. T. Dastjerd, A. Valibeik, M. Karimi, M. R. Hamblin, *Nano Today* **2020**, *34*, 100914.

[9] a) E. Fleige, M. A. Quadir, R. Haag, *Adv. Drug Delivery Rev.* **2012**, *64*, 866; b) H. Wang, Q. Huang, H. Chang, J. Xiao, Y. Cheng, *Biomater. Sci.* **2016**, *4*, 375; c) N. Li, Z. Duan, L. Wang, C. Guo, H. Zhang, Z. Gu, Q. Gong, K. Luo, *Macromol. Rapid Commun.* **2021**, *42*, 2100111.

[10] a) Y. Cheng, L. Zhao, Y. Li, T. Xu, *Chem. Soc. Rev.* **2011**, *40*, 2673; b) P. Laskar, S. Somani, N. Altwaijry, M. Mullin, D. Bowering, M. Warzecha, P. Keating, R. J. Tate, H. Y. Leung, C. Dufes, *Nanoscale* **2018**, *10*, 22830.

[11] D. Zhong, H. Wu, Y. Wu, Y. Li, X. Xu, J. Yang, Z. Gu, *Nanoscale* **2019**, *11*, 15091.

[12] a) B. Zheng, F. Wang, S. Dong, F. Huang, *Chem. Soc. Rev.* **2012**, *41*, 1621; b) W. Cui, J. Li, G. Decher, *Adv. Mater.* **2016**, *28*, 1302; c) W. C. Geng, J. L. Sessler, D. S. Guo, *Chem. Soc. Rev.* **2020**, *49*, 2303; d) A. I. Carbajo-Gordillo, J. López-Fernández, J. M. Benito, J. L. Jiménez Blanco, M. L. Santana-Armas, G. Marcelo, C. Di Giorgio, C. Przybylski, C. Ortiz Mellet, C. Tros de Ilarduya, F. Mendicuti, J. M. García Fernández, *Macromol. Rapid Commun.* **2022**, *43*, 2200145.

[13] a) U. Rauwald, O. A. Scherman, *Angew. Chem. Int. Ed. Engl.* **2008**, *47*, 3950; b) U. Rauwald, J. del Barrio, X. J. Loh, O. A. Scherman, *Chem. Commun.* **2011**, *47*, 6000; c) H. Mousazadeh, Y. Pilehvar-Soltanahmadi, M. Dadashpour, N. Zarghami, *J. Control. Release* **2021**, *330*, 1046; d) Z. Wang, C. Sun, K. Yang, X. Chen, R. Wang, *Angew. Chem. Int. Ed. Engl.* **2022**, *61*, e202206763.

[14] W. S. Jeon, E. Kim, Y. H. Ko, I. Hwang, J. W. Lee, S. Y. Kim, H. J. Kim, K. Kim, *Angew. Chem. Int. Ed. Engl.* **2004**, *44*, 87.

[15] H. J. Kim, J. Heo, W. S. Jeon, E. Lee, J. Kim, S. Sakamoto, K. Yamaguchi, K. Kim, *Angew. Chem. Int. Ed. Engl.* **2001**, *40*, 1526.

[16] a) X. Cai, J. Hu, J. Xiao, Y. Cheng, *Expert Opin. Ther. Pat.* **2013**, *23*, 515; b) Q. Hu, W. Wu, M. Wang, S. Shao, P. Jin, Q. Chen, H. Bai, X. Zhao, J. Huang, J. Wang, G. Tang, T. Liang, *J. Control. Release* **2020**, *317*, 67.

[17] C. Song, M. Shen, J. Rodrigues, S. Mignani, J.-P. Majoral, X. Shi, *Coord. Chem. Rev.* **2020**, *421*, 213463.

[18] D. Wu, Y. Li, J. Yang, J. Shen, J. Zhou, Q. Hu, G. Yu, G. Tang, X. Chen, *ACS. Appl. Mater. Interfaces* **2017**, *9*, 44392.

[19] L. J. Fox, R. M. Richardson, W. H. Briscoe, *Adv. Colloid Interface Sci.* **2018**, *257*, 1.

[20] a) K. Wang, Q. D. Hu, W. Zhu, M. M. Zhao, Y. Ping, G. P. Tang, *Adv. Funct. Mater.* **2015**, *25*, 3380; b) D. Luong, P. Kesharwani, R. Deshmukh, M. C. I. Mohd Amin, U. Gupta, K. Greish, A. K. Iyer, *Acta. Biomater.* **2016**, *43*, 14; c) P. Laskar, S. Somani, M. Mullin, R. J. Tate, M. Warzecha, D. Bowering, P. Keating, C. Irving, H. Y. Leung, C. Dufes, *Biomater. Sci.* **2021**, *9*, 1431.

[21] J. Che, C. I. Okeke, Z. B. Hu, J. Xu, *Curr. Pharm. Des.* **2015**, *21*, 1598.

[22] V. Leiro, A. P. Spencer, N. Magalhaes, A. P. Pego, *Biomaterials* **2022**, *281*, 121356.

[23] O. Boussif, F. Lezoualc'h, M. A. Zanta, M. D. Mergny, D. Scherman, B. Demeneix, J. P. Behr, *Proc. Natl. Acad. Sci.* **1995**, *92*, 7297.

Supplementary Information

Stimuli-responsive dendritic supramolecular vector for tumor-specific gene delivery

Xumei Ouyang[1,2,3,#], Dongruo Gao[1,4,#], Jie Shen[1,3,5,*] , Yichen Zhou[1] , Ying Gao[1,3], Yuanyuan Lv[1,3,4], Qiwen Wang[6,*], Guocan Yu[7,*], Paul K. Chu[5,*]

[1] Key Laboratory of Novel Targets and Drug Study for Neural Repair of Zhejiang Province, School of Medicine, Hangzhou City University, Hangzhou 310015, China

[2] Guangdong Provincial Key Laboratory of Tumor Interventional Diagnosis and Treatment, Zhuhai Institute of Translational Medicine Zhuhai People's Hospital Affiliated with Jinan University, Jinan University, Zhuhai, 519000, Guangdong, China

[3] Institute of Pharmaceutics, College of Pharmaceutical Sciences, Zhejiang University, Hangzhou 310058, China

[4] College of Chemical and Biological Engineering, Zhejiang University, Zhejiang, Hangzhou 310027, China

[5] Department of Physics, Department of Materials Science and Engineering, and Department of Biomedical Engineering, City University of Hong Kong, Tat Chee Avenue, Kowloon, Hong Kong, China

[6] Department of Cardiology, The First Affiliated Hospital, Zhejiang University School of Medicine, Hangzhou 310003, China

[7] Key Laboratory of Bioorganic Phosphorus Chemistry & Chemical Biology, Department of Chemistry, Tsinghua University, Beijing 100084, China.

[#] These authors contributed equally to this work.

***** Corresponding authors:

Jie Shen, PhD

[1] Key Laboratory of Novel Targets and Drug Study for Neural Repair of Zhejiang Province, School of Medicine, Hangzhou City University, Hangzhou 310015, China

E-mail: shenj@zucc.edu.cn

Qiwen Wang, MD

[6]Department of Cardiology, The First Affiliated Hospital, Zhejiang University School of Medicine, Hangzhou 310003, China

E-mail: wangqiwen@zju.edu.cn

Prof. Guocan Yu, PhD

[7] Key Laboratory of Bioorganic Phosphorus Chemistry & Chemical Biology, Department of Chemistry, Tsinghua University, Beijing 100084, China.

E-mail: guocanyu@mail.tsinghua.edu.cn.

Prof. Paul K Chu, PhD

[5] Department of Physics, Department of Materials Science and Engineering, and Department of Biomedical Engineering, City University of Hong Kong, Tat Chee Avenue, Kowloon, Hong Kong, China

Tel: 852-34427724; Fax: 852-34420542

E-mail: paul.chu@cityu.edu.hk.

1. Materials

2. Synthesis of the DN segment

3. Synthesis of the VP segment

4. Linear fit schemes

5. Particle size of DNCVP under the reductive conditions

6. Protein absorption study

7. Cellular uptake for free siRNA

8. Fluorescence quantification results

9. Frozen section of tumors and kidneys

1. Materials

Tert-Butyl acrylate, 3-hydroxytriazolo[4,5-b]pyridine (HOAt), N-boc-ethylenediamine, 1-ethyl-(3-dimethylaminopropyl)carbodiimide hydrochloride (EDCI), nickel chloride hexahydrate ($NiCl_2 \cdot 6H_2O$), trifluoroacetic acid (TFA), and 4-dimethylaminopyridine (DMAP) were purchased from Macklin and used without further purification. Benzyltrimethylammonium hydroxide (Triton-B) and 2-hydrazinoethanol (2-HEH) were provided by Aladdin and used without further purification. mPEG-propionaldehyde (mPEG-ALD, MW 2000) and mPEG-NH_2 were purchased from Shanghai Yare Biotech and used without further purification. Solvents such as dimethyl sulfoxide (DMSO), dichloromethane, and so on were purchased from Tianjin Yongda and 1,1'-Carbonyldiimidazole (CDI) was obtained from Shanghai Yuanye Biotech. Dialysis bag was purchased from Viskase.

2. Synthesis of the DN segment

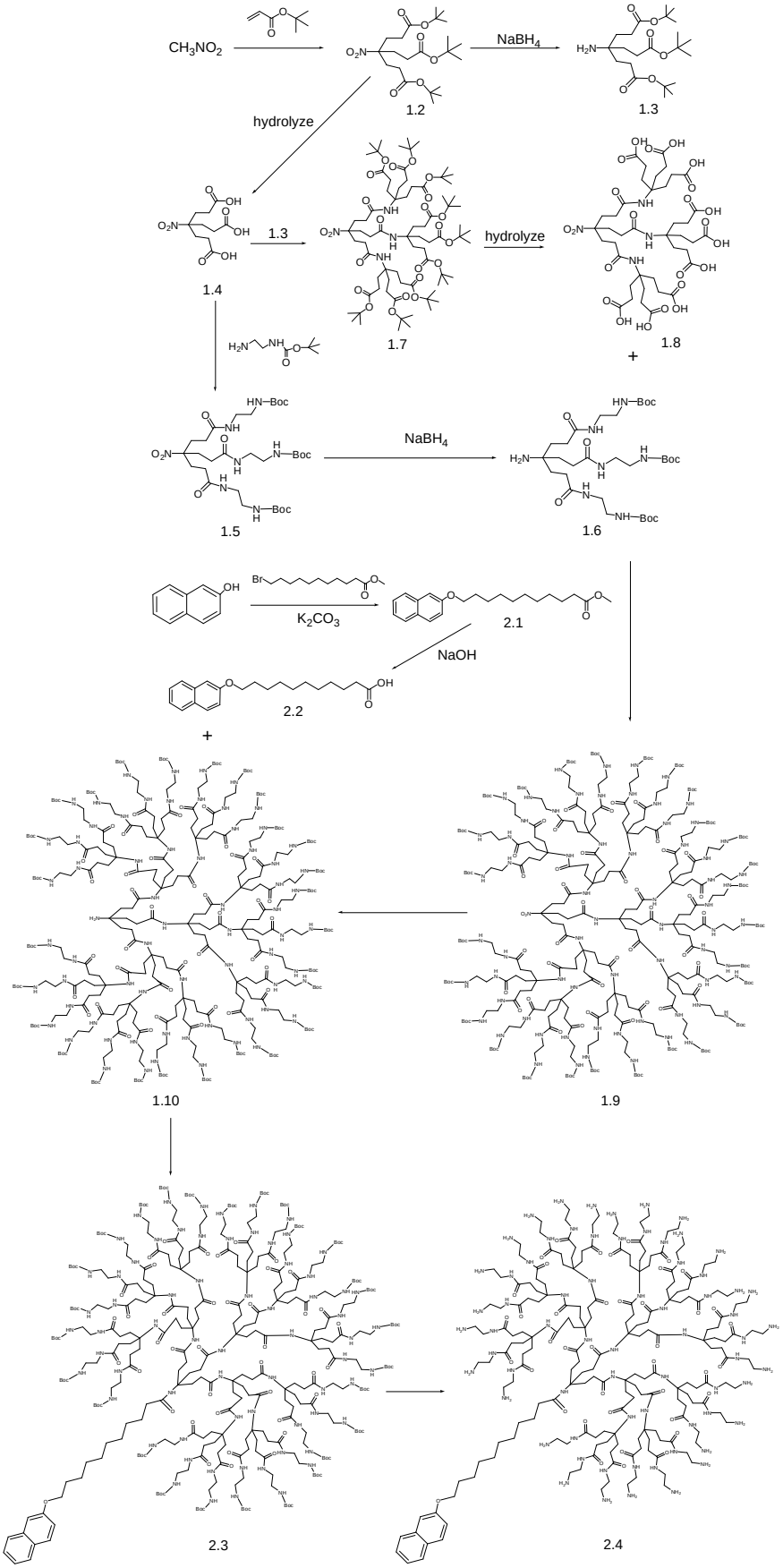
CH3NO2
NaBH4
1.2
1.3
hydrolyze
1.4
1.7
1.8
hydrolyze
NaBH4
1.5
1.6
K2CO3
2.1
NaOH
2.2
1.10
1.9
2.3
2.4

Synthesis of compounds **1.2**, **1.5**, **1.6** is according to the previous work.[1]

Synthesis of compound 1.3. $NiCl_2 \cdot 6H_2O$ (237.7 mg, 1 mmol) and $NaBH_4$ (189.4 mg, 5 mmol) were added at 0 ºC to a solution containing compound 1.2 (445.6 mg, 1 mmol) in MeOH (10 mL). The mixture was stirred at 0 ºC for 15 min and then at room temperature for 3 h before quenching by dropwise addition of 1 mol/L hydrochloric acid. Saturated sodium bicarbonate was then added dropwise until the pH was 9. After methanol was evaporated, the aqueous layer was extracted with ethyl acetate 3 times. The combined organic layers were washed with saturated aqueous sodium chloride and dried with anhydrous Na_2SO_4. Compound 1.3 was obtained after removing the solvent at a reduced pressure (95.2% yield). The ^1H NMR conditions were: 400 MHz, $CDCl_3$, room temperature; δ (ppm): 2.26-2.23 (m, 6H), 1.63-1.60 (m, 6H), 1.44 (s, 27H).

Synthesis of compound 1.4. The solution containing compound 1.2 (445.6 mg, 1 mmol) in formic acid (96%) was stirred at 40 ºC for 12 h. After it was evaporated at reduced pressure to remove most of the formic acid, the residue was dissolved in methanol. IT was evaporated at reduced pressure to remove methanol and remaining formic acid (×3) to form compound 1.4 (98.8% yield).

Synthesis of compound 1.7. To the solution containing compound 1.3 (1.37g, 3.3 mmol), compound 4 (277.2 mg, 1.0 mmol), HOAt (490 mg, 3.6 mmol), and Et_3N (1.4 mL, 10 mmol) in CH_2Cl_2 (20 mL), EDCI (1.01 g, 6 mmol) were added at 0 ºC. The mixture was stirred at 0 ºC for 0.5 h and then at room temperature for 3 h. Saturated

aqueous sodium chloride (30 mL) was added afterwards and the organic layer was washed successively with 1.0 mol/L hydrochloric acid (30 mL), saturated aqueous sodium bicarbonate (30 mL), and saturated aqueous sodium chloride (30 mL). The organic layer was dried with anhydrous Na_2SO_4 and after evaporation at reduced pressure, compound **1.7** was obtained (92.3% yield). The ^{1}H NMR conditions were: 400 MHz, $CDCl_3$, room temperature; δ (ppm): 5.65 (s, 3H), 2.31-2.08 (s, 30H), 2.00-1.78 (m, 18H), 1.44 (s, 81H).

Synthesis of compound 1.8. The solution containing compound 1.7 (1.47 g, 1 mmol) in formic acid (96%) was stirred at 45 ºC for 36 h and evaporated at reduced pressure to remove most of the formic acid. The residue was dissolved in methanol and was evaporated at reduced pressure to remove methanol and remaining formic acid (×3). Compound 1.8 was obtained (94.6% yield). The ^{1}H NMR conditions were: 400 MHz, DMSO-*d6*, room temperature; δ (ppm): 12.38 (s, 6H), 7.71 (s, 6H), 2.34-2.02 (s, 30H), 1.85-1.60 (dd, 18H).

Synthesis of compound 1.9. To the solution containing compound 1.8 (1.01g, 1 mmol), compound 6 (8.09 g, 12 mmol), HOAt (1.63 g, 12 mmol), and Et_3N (5.6 mL, 40 mmol) in DMF (50 mL), EDCI (4.60 g, 24 mmol) were added at 0 ºC. The mixture was stirred at 0 ºC for 0.5 h and then at room temperature for 48 h. It was dialyzed against water in a dialysis bag (MW=2000 Da) for 24 h and dialyzed against MeOH twice to obtain compound 1.9 after evaporation at reduced pressure (81.7% yield). The ^{1}H NMR conditions were: 400 MHz, DMSO-*d6*, room temperature; δ (ppm): 7.82(s, 27H), 7.38-7.15 (d, 10H), 6.76 (s, 24H), 6.39 (s, 3H), 3.12-2.89 (d, 108H), 2.18-

1.88 (d, 84H), 1.89-1.56 (d, 72H), 1.36 (s, 243H).

Synthesis of compound 1.10. To a solution consisting of compound 1.9 (614.0 mg, 0.1 mmol) in MeOH (20 mL), $NiCl_2 \cdot 6H_2O$ (237.7 mg, 1 mmol) and $NaBH_4$ (75.66 mg, 2 mmol) were added at 0ºC. The mixture was first stirred at 0ºC for 0.5 h and then at room temperature for 12 h. It was quenched by dropwise addition of 1 mol/L hydrochloric acid. Afterwards, saturated sodium bicarbonate was added to obtain a pH of 9. After methanol was removed by evaporation, the aqueous layer was extracted with ethyl acetate 3 times. After evaporation at reduced pressure, the residue was purified by silica gel flash column chromatography (CH_2Cl_2/ petroleum ether = 2/1) to produce compound 1.10 (65.5% yield). The ^{1}H NMR conditions were: 400 MHz, DMSO-*d6*, room temperature) δ (ppm): 7.85 (s, 27H), 7.37-7.14 (d, 10H), 6.76 (s, 24H), 6.39 (s, 3H), 3.10-2.89 (d, 108H), 2.16-1.90 (d, 78H), 1.89-1.56 (d, 78H), 1.36 (s, 243H).

The synthesis method of **compounds 2.1 and 2.2** is according to the work of Conrad.[2]

Synthesis of compound 2.3. To a solution containing compound 2.2 (56.69 mg, 0.2mmol) and Et_3N (1.4 mL, 10 mmol) in DMSO (20 mL), the solution of CDI (32.43 mg, 0.2mmol) in DMSO (10 mL) was added at 0 ºC. The mixture was stirred at 0 ºC for 0.5 h and at room temperature for 12 h. Compound 1.10 (610.8 mg, 0.1mmol) in DMSO (10 mL) was added and stirred at room temperature for 24 h. The mixture was dialyzed against water in a dialysis bag (MW = 2000 Da) for 24 h and then against ethyl acetate 2 times to produce compound 2.3 after evaporation at reduced pressure (61.9%

yield).

Synthesis of compound 2.4. Compound 2.3 (712.2 mg, 0.01 mmol)was dissolved in a mixture of TFA (10 mL) and CH_2Cl_2 (10 mL) at 0 ºC followed by stirring at room temperature for 36 h. 1 mol/L aqueous sodium hydroxide was added dropwise until the pH was 9. The mixture was dialyzed against water in a dialysis bag (MW = 2000 Da) for 24 h and freeze-dried to form compound 2.4 (89.1% yield).

3. Synthesis of the VP segment

Synthesis of compound 3.1. The solution containing bipyridine (1.57 g, 10 mmol) and CH_3I (1.33 g, 5 mmol) in CH_2Cl_2 (30 mL) was stirred at 40ºC for 2 h. It was filtered at room temperature and the residue was washed with ethyl acetate. The obtained solid was recrystallized and dried to form compound 3.1 which was a yellow powder (43.1% yield).

Synthesis of compound 3.2. The solution consisting of compound 3.1 (298.1 mg, 1 mmol) and 11-bromoundecanoic acid (1.85 g, 13 mmol) in CH_3CN (30 mL) was stirred at 95 ºC for 24 h. The mixture was filtered at room temperature and the residue was washed with methylbenzene. The solid was dried to form compound 3.2 (72.7% yield). The ^1H NMR conditions were: 400 MHz, D_2O, room temperature; δ (ppm): 9.02-8.90 (dd, 4H), 8.44-8.37 (t, 4H), 4.63-4.57 (t, 2H), 4.38 (s, 3H), 2.25-2.19 (t, 2H), 2.00-1.91 (m, 2H), 1.48-1.32 (m, 2H), 1.27-1.12 (m, 12H).

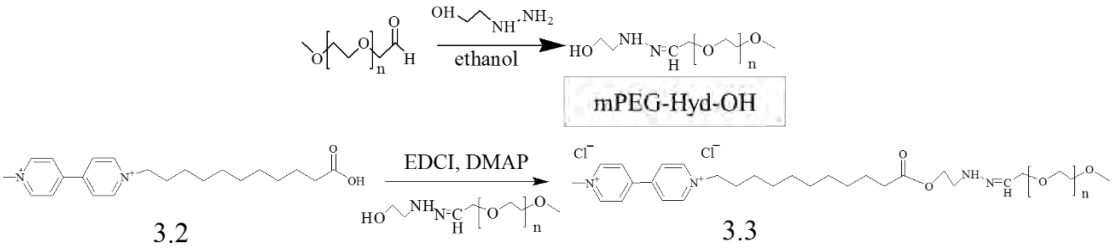

Synthesis of compound 3.3. Synthesis of mPEG-Hyd-OH was according to the work of Laouini.[3] To the solution containing compound 3.2 (39.4 mg, 0.07 mmol), EDCI (95.8 mg, 0.5 mmol) and Et_3N (1.4 mL, 10 mmol) in DMSO, a solution of DMAP (32.43 mg, 0.2mmol) in DMSO (10 mL) was added. After 0.5 h, Et_3N was added dropwise to reach a pH of 9. The solution of mPEG-Hyd-OH (103.7 mg, 0.05 mmol) in DMSO (5 mL) was added and stirred at room temperature for 24 h in the dark. It wsa then dialyzed against water in a dialysis bag (MW = 2000 Da) for 24 h and freeze-dried to form compound 3.3 (21.3% yield).

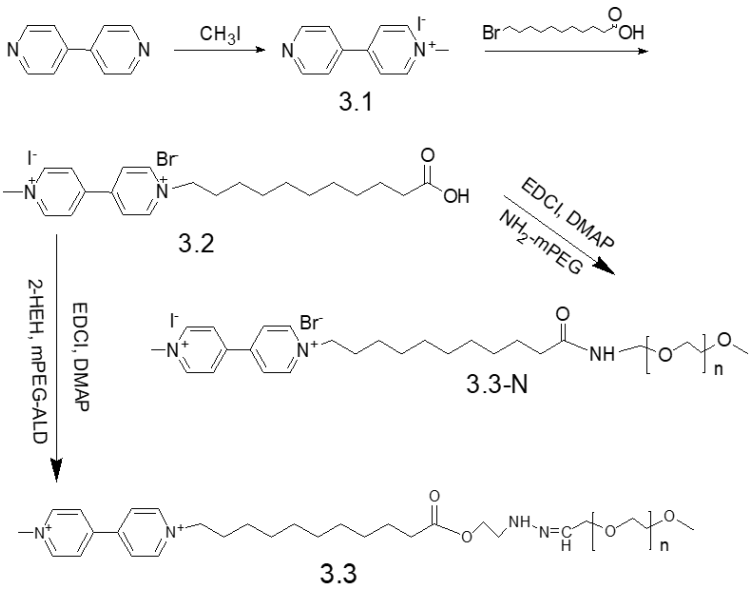

Synthesis of compound 3.3-N. The solution comprising compound 3.2 (56.3 mg,

0.1 mmol), EDCI (95.8 mg, 0.5 mmol) and NHS (57.5 mg, 0.5 mmol) in H_2O was stirred at room temperature for 0.5 h in the dark and then Et_3N was added dropwise until the pH became 8. The solution of mPEG-NH_2 (75 mg, 0.1 mmol) in H_2O (5 mL) was added and stirred at room temperature for 24 h in darkness. It was dialyzed against water in a dialysis bag (MW = 2000 Da) for 24 h and freeze-dried to produce compound 3.3-N (31.6% yield).

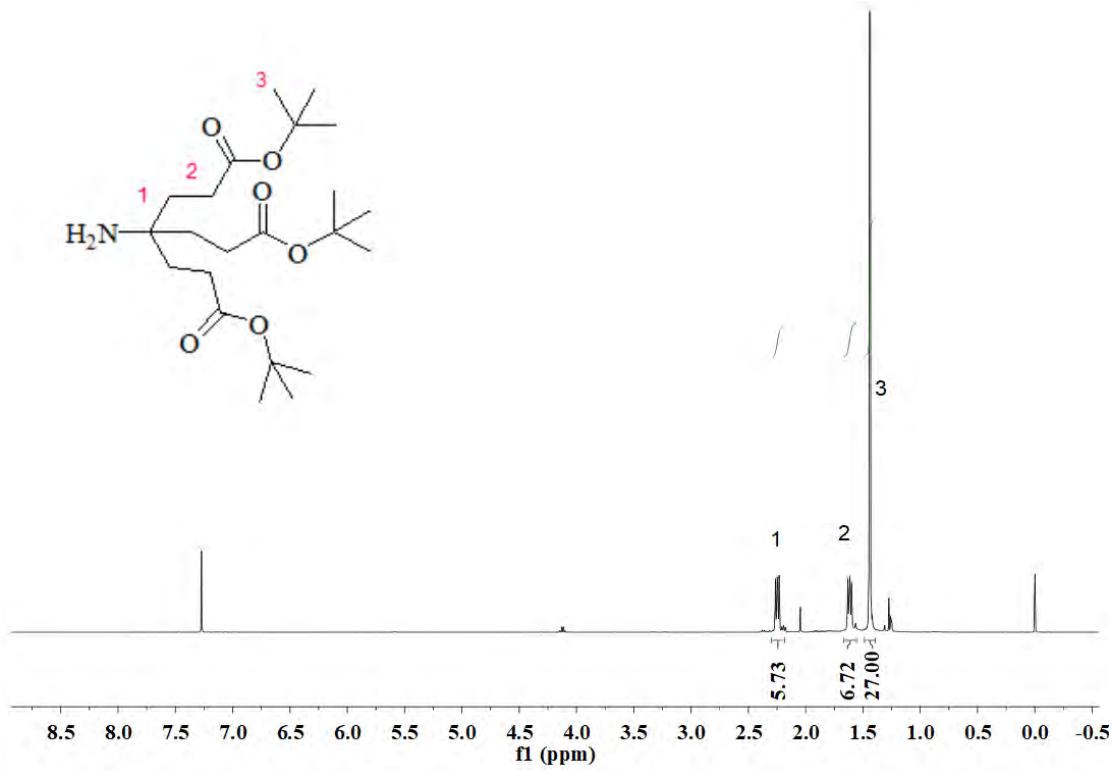

Figure S1. ^{1}H NMR spectrum (400 MHz, $CDCl_3$, room temperature) of compound 1.3.

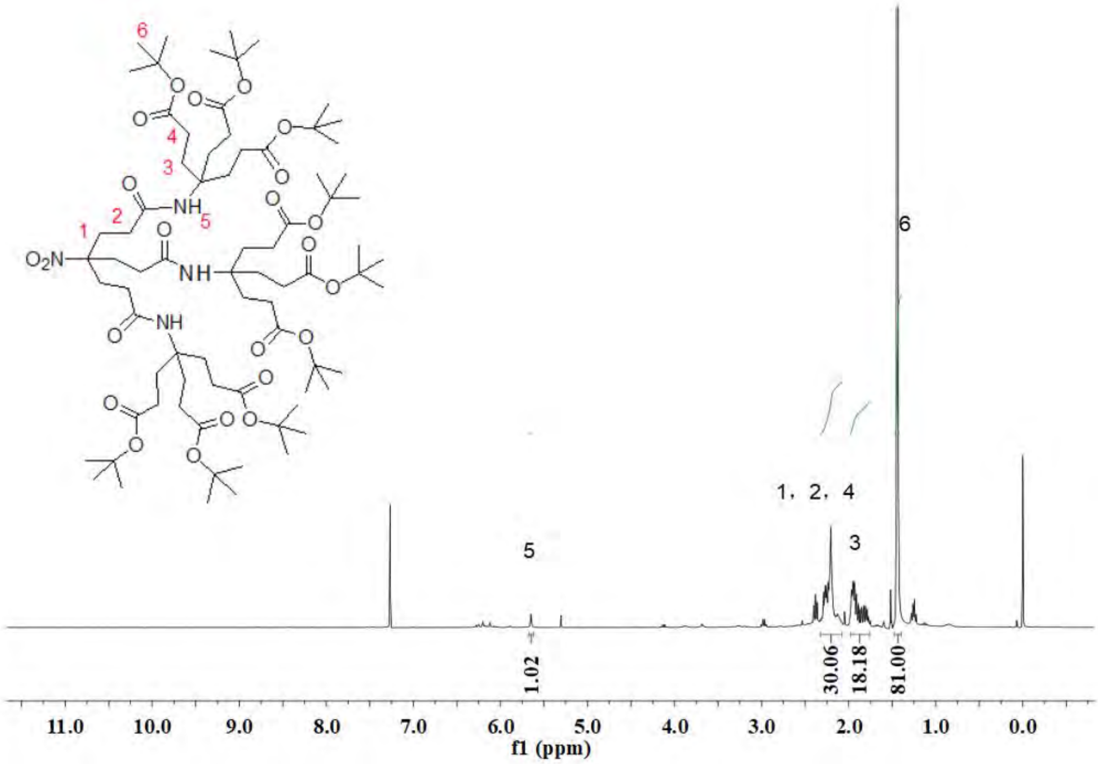

Figure S2. ^{1}H NMR spectrum (400 MHz, $CDCl_3$, room temperature) of compound 1.7.

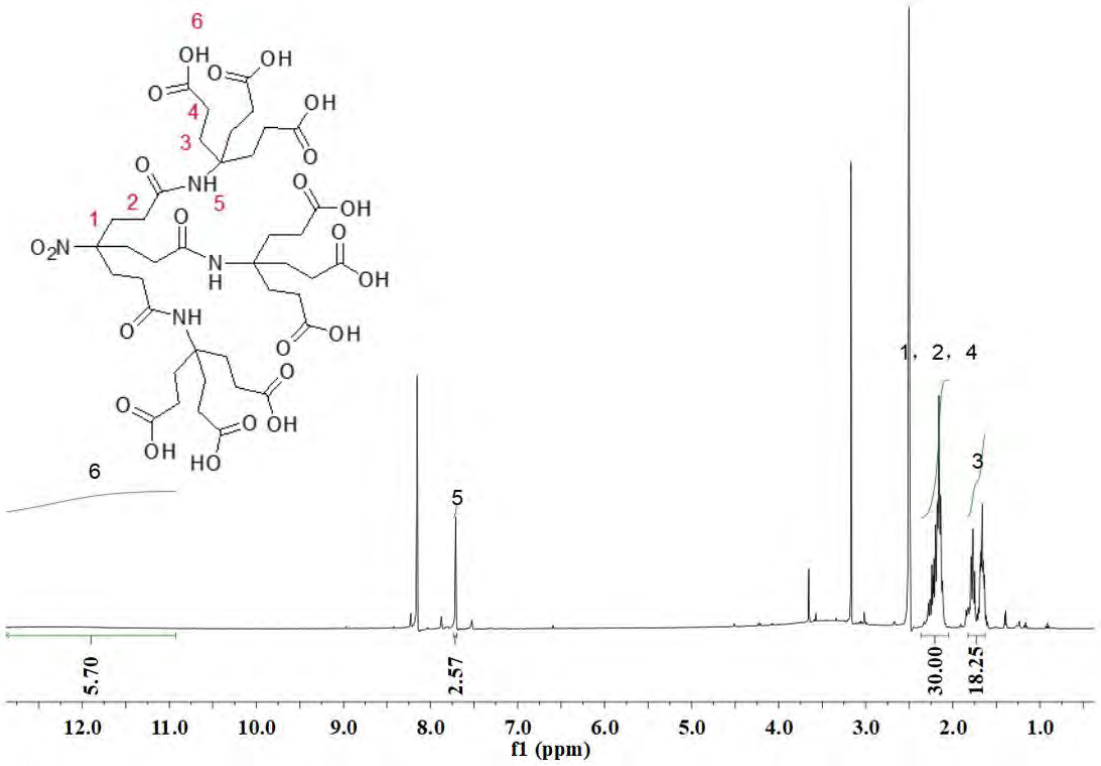

Figure S3. ^{1}H NMR spectrum (400 MHz, DMSO-*d6*, room temperature) of compound 1.8.

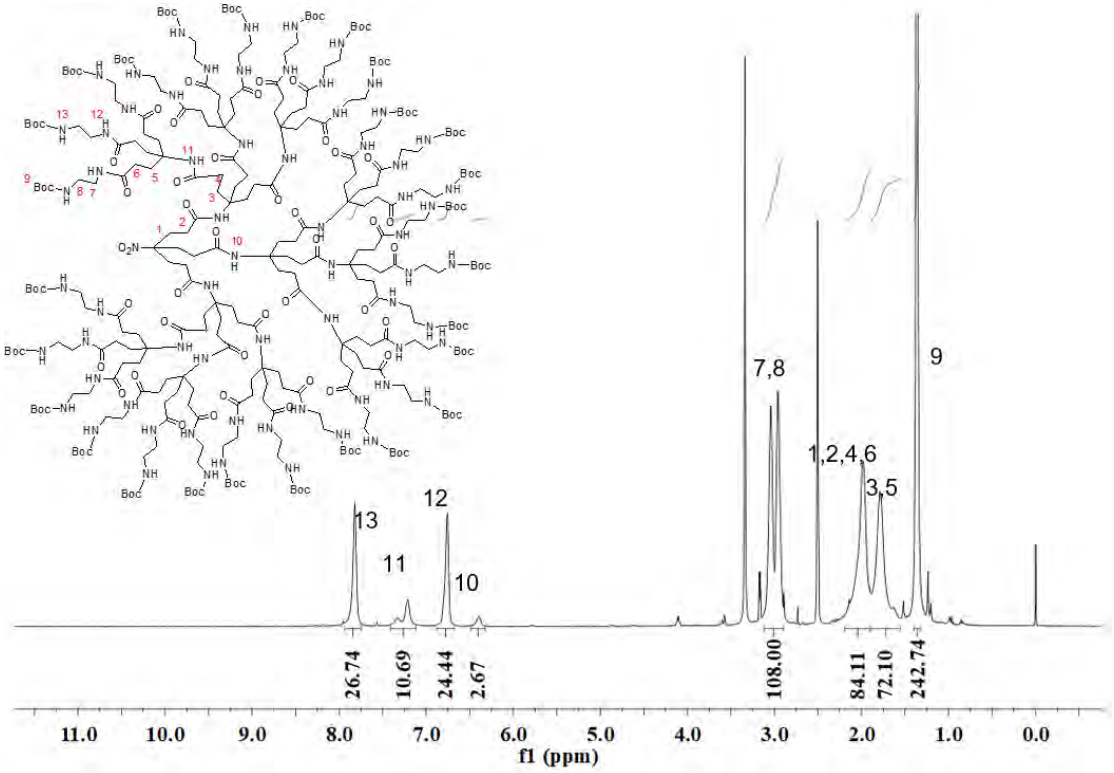

Figure S4. ^{1}H NMR spectrum (400 MHz, DMSO-*d6*, room temperature) of compound 1.9.

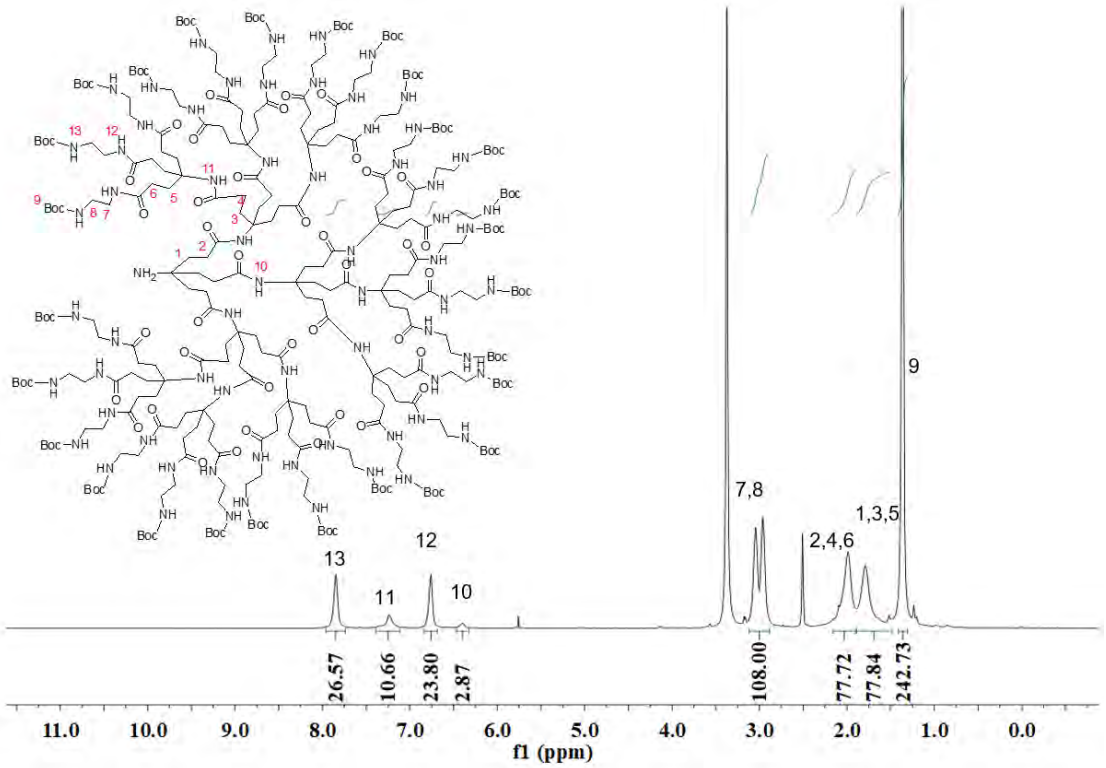

Figure S5. ^{1}H NMR spectrum (400 MHz, DMSO-*d6*, room temperature) of compound 1.10.

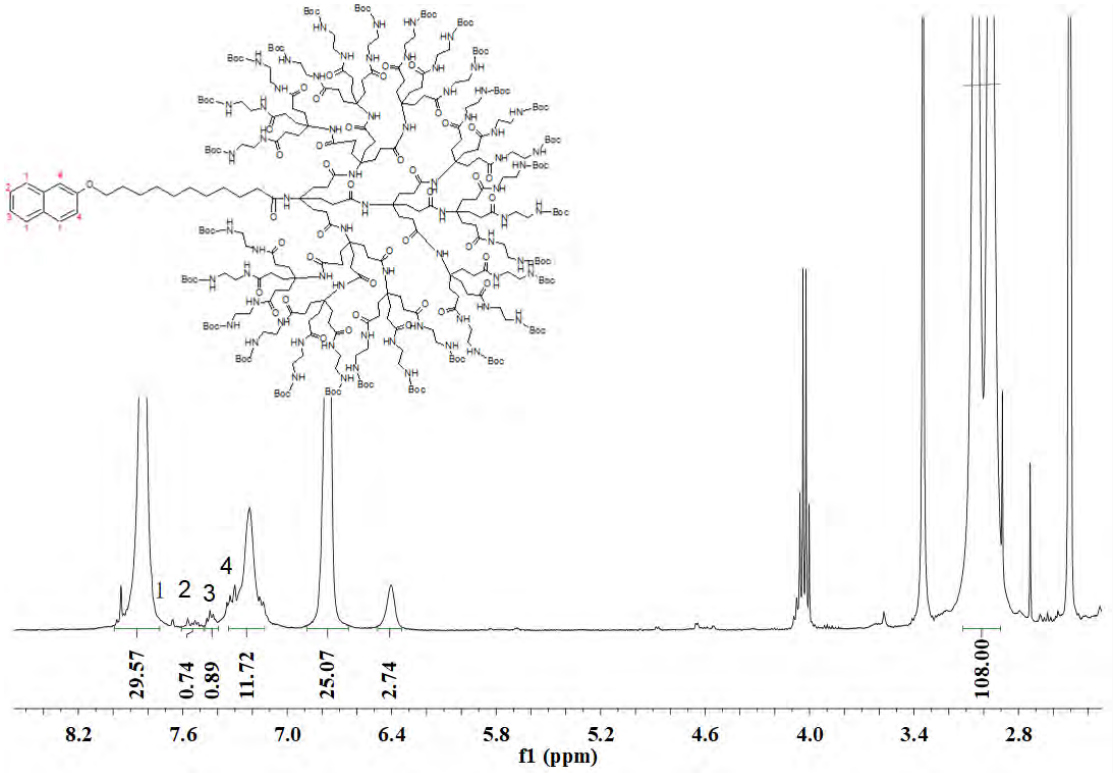

Figure S6. ^{1}H NMR spectrum (400 MHz, DMSO-*d6*, room temperature) of compound 2.3.

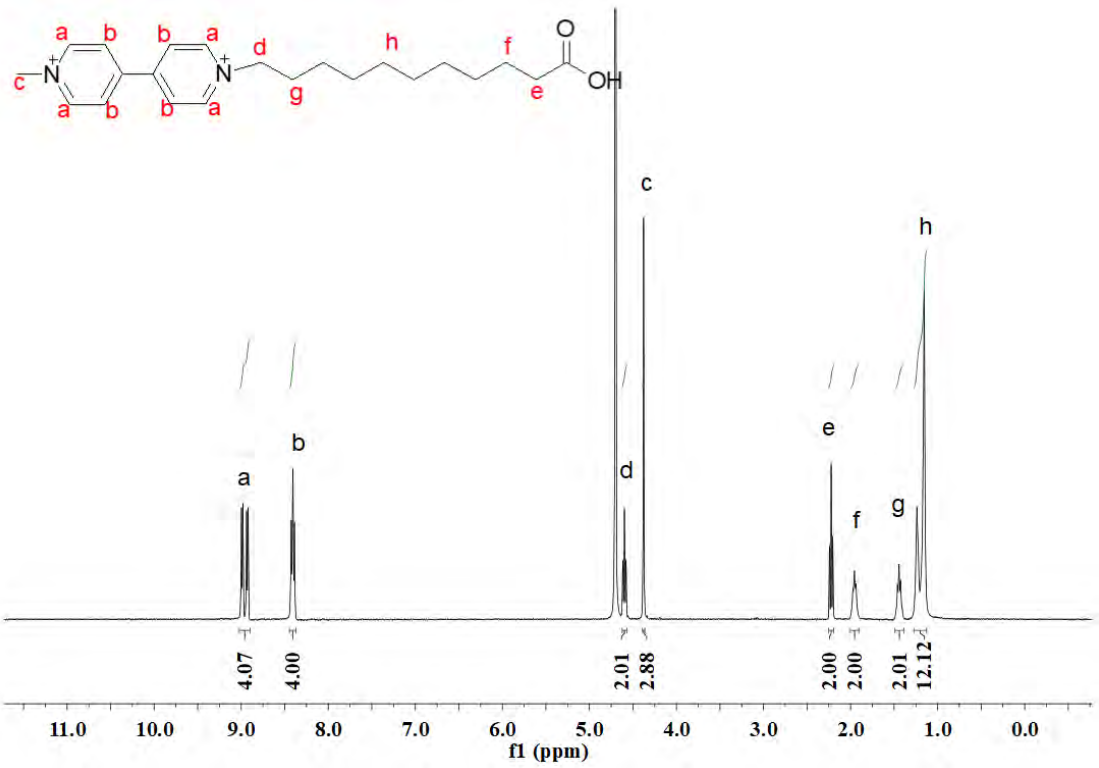

Figure S7. ^{1}H NMR spectrum (400 MHz, D_2O, room temperature) of compound 3.2.

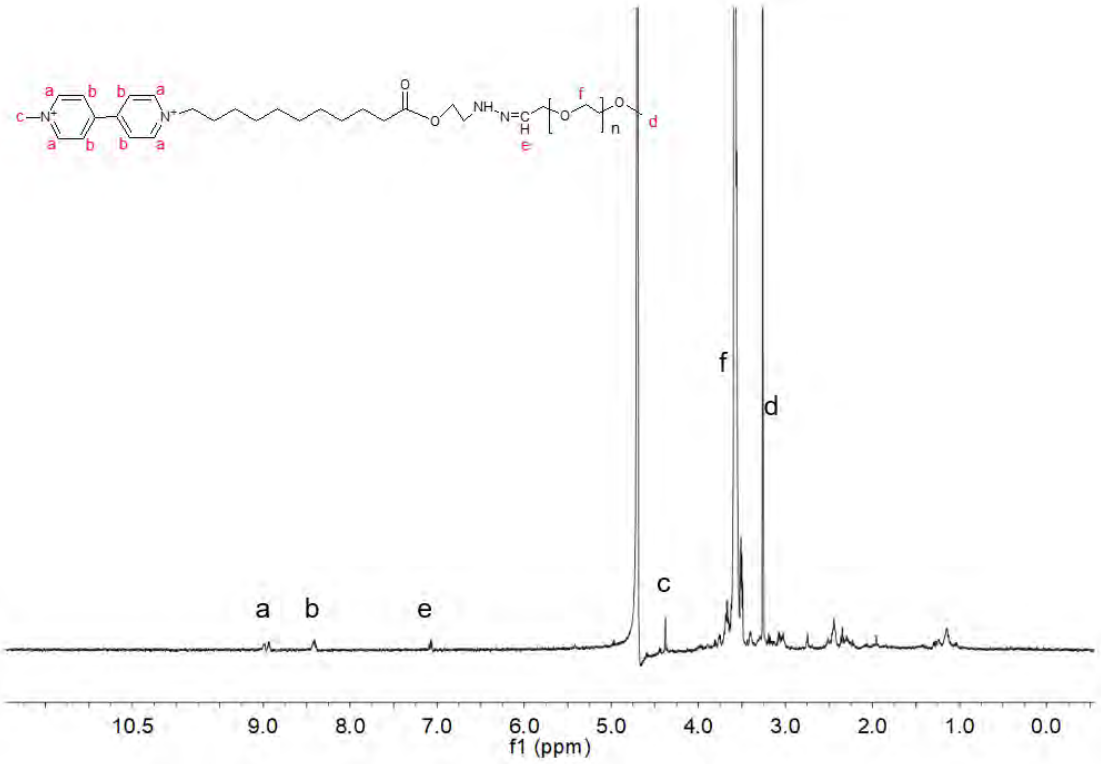

Figure S8. ^{1}H NMR spectrum (400 MHz, D_2O, room temperature) of compound 3.3.

4. Linear fittings

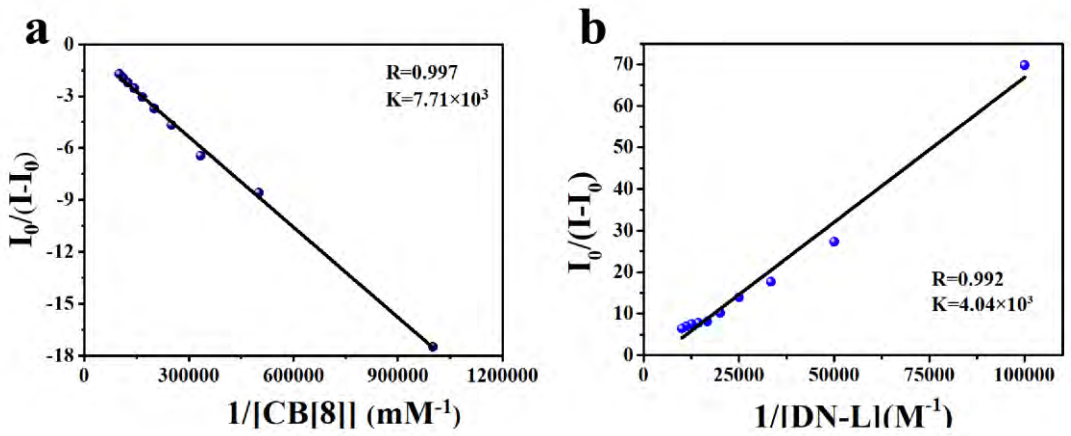

Figure S9. (a) Linear fit of $I_0/(I-I_0)$ and 1/[CB[8]] for VP-L titrated with CB[8] and (b) Linear fit of $I_0/(I-I_0)$ and 1/[DN-L] for VP-L/CB[8] titrated with DN-L.

5. Particle size of DNCVP under the reduction conditions

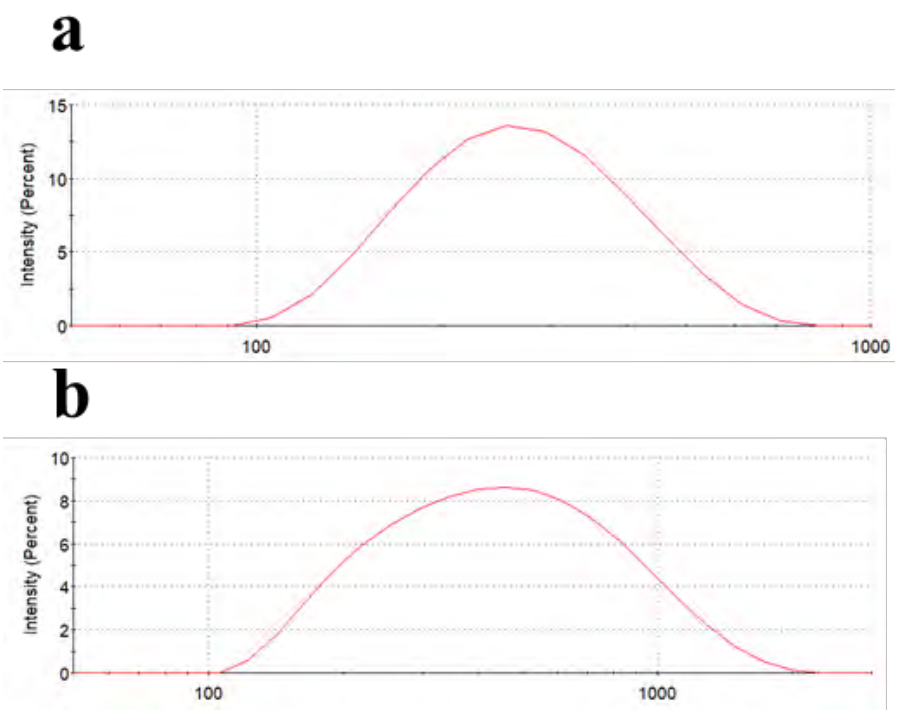

Figure S10. Particle size distributions of DNCVP/siRNA at N/P = 20 (a) before and (b) after the treatment with reduced $Na_2S_2O_5$.

6. Protein absorption

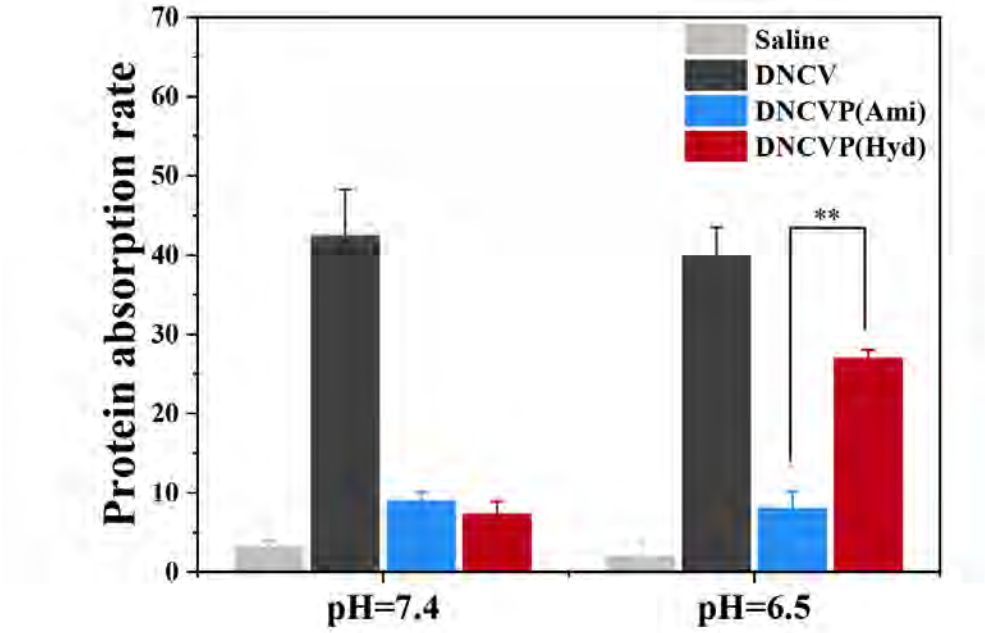

Figure S11. Adsorption of bovine serum albumin of DNCV, DNCVP(Ami), and DNCVP(Hyd) at different pH (n = 3, $^{**}p < 0.01$).

7. Cellular uptake for free siRNA

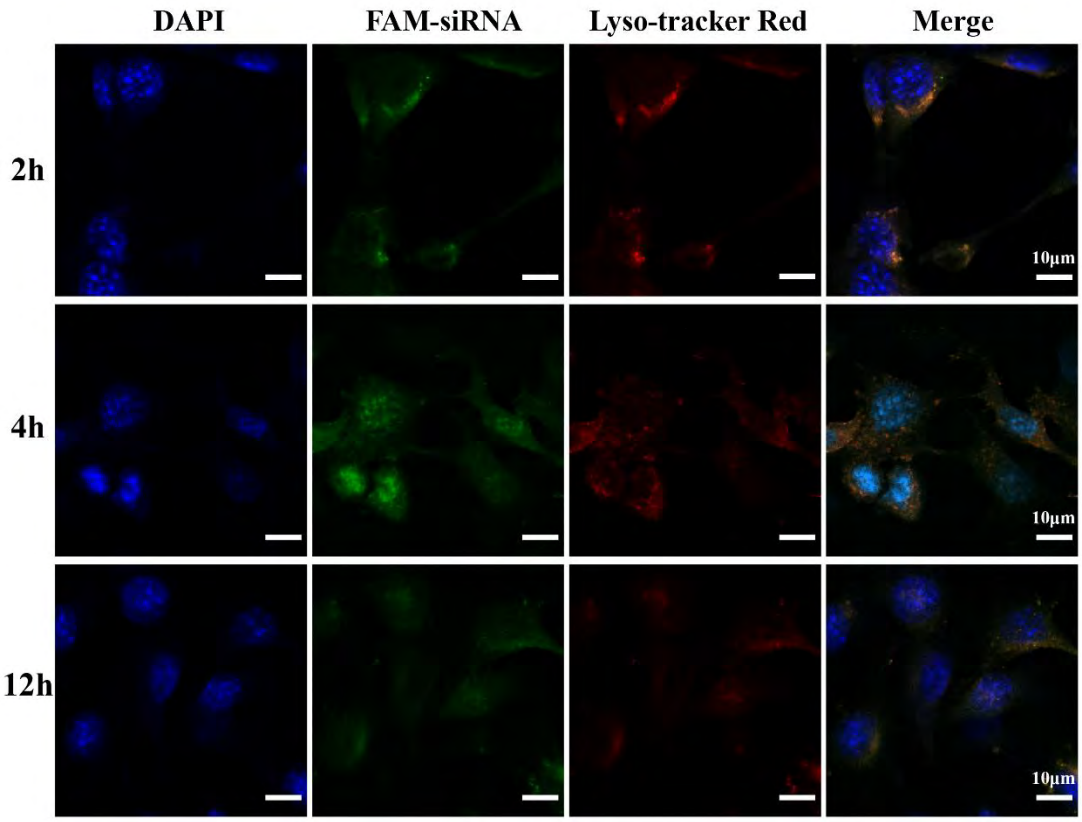

Figure S12 Fluorescent confocal microscopy images of B16F10 treated with free FAM-siRNA for 2, 4, and 12 h (scale bars =10 μm).

8. Fluorescence quantification results

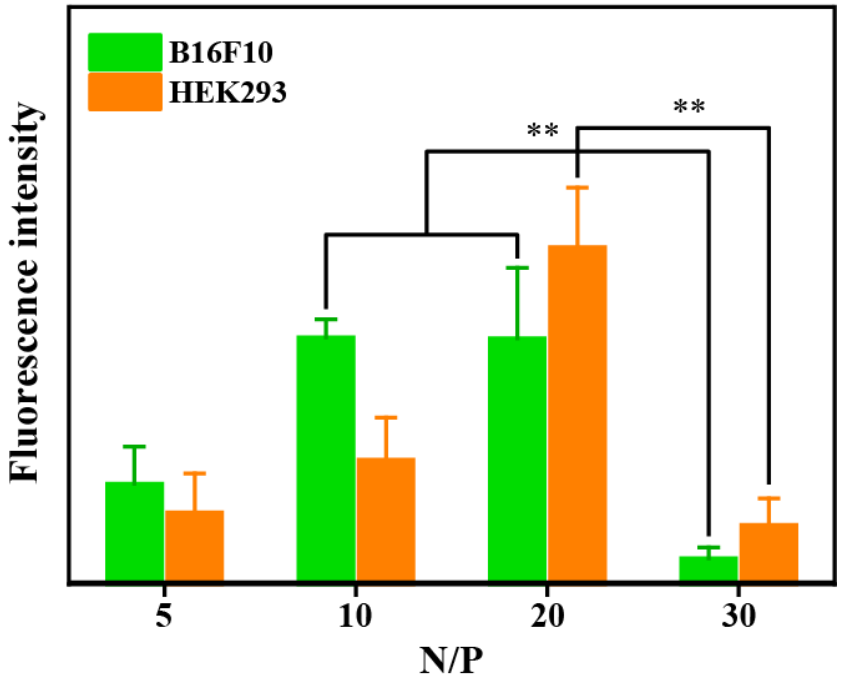

Figure S13 Quantitative fluorescence intensities from B16F10 and HEK293 cells treated with DNCVP/pEGFP for different N/P (n=3).

9. Frozen section of tumors and kidneys

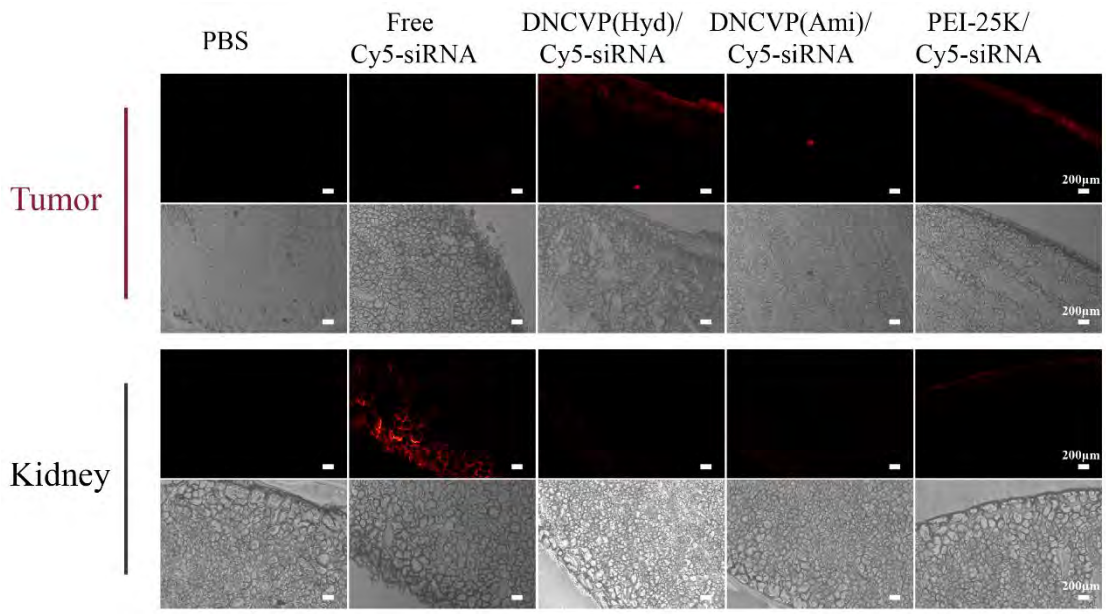

Figure S14 Fluorescence and optical images of tumor sites and kidneys 24 h after injection of PBS, free Cy5-siRNA, DNCVP(Ami)/Cy5-siRNA, DNCVP(Hyd)/Cy5-siRNA, PEI-25K/Cy5-siRNA via the tail vein (scale bars = 200 μm).

References

[1] K. Wang, Q. Hu, W. Zhu, M. Zhao, Y. Ping, G. Tang, *Adv. Funct. Mater.* **2015**, *25*, 3380.

[2] J. C. Conrad, J. Kong, B. N. Laforteza, D. W. MacMillan, *J. Am. Chem. Soc.* **2009**, *131*, 11640.

[3] A. Laouini, K. P. Koutroumanis, C. Charcosset, S. Georgiadou, H. Fessi, R. G. Holdich, G. T. Vladisavljević, *ACS Appl. Mater. Interfaces* **2013**, *5*, 8939.